10

Ferket, H., S. Ortuño-Arzate, F. Roure, and R. Swennen, 2003, Lithologic control on matrix porosity in shallow-marine Cretaceous reservoir limestones: A study of the Peñuela reservoir outcrop analogue (Cordoba Platform, Southeastern Mexico), *in* C. Bartolini, R. T. Buffler, and J. Blickwede, eds., The Circum-Gulf of Mexico and the Caribbean: Hydrocarbon habitats, basin formation, and plate tectonics: AAPG Memoir 79, p. 283–304.

Lithologic Control on Matrix Porosity in Shallow-marine Cretaceous Reservoir Limestones: A Study of the Peñuela Reservoir Outcrop Analogue (Cordoba Platform, Southeastern Mexico)

H. Ferket
Fysico-chemische Geologie, K. U. Leuven, Heverlee, Belgium

S. Ortuño-Arzate
Instituto Mexicano del Petróleo, México, D.F., México

F. Roure
Institut Français du Pétrole, Rueil-Malmaison Cedex, France

R. Swennen
Fysico-chemische Geologie, K. U. Leuven, Heverlee, Belgium

ABSTRACT

Selectively oil-impregnated limestones from the Upper Cretaceous Guzmantla Formation, outcropping in the Cordoba Platform of eastern Mexico, were studied to determine the factors controlling the porosity and hydrocarbon distribution and to reconstruct the fluid-flow history.

In the two exposed upward-coarsening (i.e., upward-shoaling) sequences, three limestone lithotypes were distinguished, based on sedimentary, diagenetic, and oil-impregnation characteristics. Lithotype I is comprised of mud-dominated low-energy deposits, which have been affected strongly by compaction. These strata are oil impregnated only along stylolites. Lithotype II consists of bioclastic wackestones to packstones deposited in an open-platform lagoonal environment. This lithotype is pervasively oil impregnated. The preservation of porosity is explained by the development of framework-stabilizing, interparticular, early diagenetic (marine and meteoric) calcite cements. Furthermore, secondary porosity was created after layer-parallel shortening (LPS), when LPS-related structures

were opened during subsequent folding of the strata. Lithotype III consists of bioclastic shoal grainstones that have been cemented pervasively during early-marine and later meteoric diagenesis, occluding primary porosity and thus preventing oil impregnation.

However, Lithotype III strata display an important modern macroporosity, related to a telogenetic phase of karst development that postdates oil migration. Due to the lack of driving forces, the oil did not migrate into these karst-related pores. In Lithotype II, the presence of oil reduced the effective porosity and hindered further fluid migration. Lithotype II strata thus were less affected by the telogenetic karstification. Lithotype I was less affected because of the completely compacted matrix. This late-stage (postoil migration) dissolution phase is not important in this specific history, but it may be very important in similar deposits in the subsurface, where it can enhance appreciably the reservoir capacity.

Factors controlling porosity-permeability are, first, the sedimentary environment, which influenced early and, thus also, later diagenetic evolution. Furthermore, stylolite development (compactional as well as tectonic), which exerts a negative effect on porosity-permeability because of pressure-dissolution and related matrix cementation, also is an important factor. However, because of tectonic opening of some of the stylolites and channelling of meteoric fluids, with porosity development as a result, these stylolites also may increase permeability and total porosity. Finally, fracturing of the strata, whereby tectonic opening and/or cementation can take place, exerts a major influence on reservoir characteristics.

INTRODUCTION

Exploration for hydrocarbons in carbonate reservoirs requires a good understanding of the factors controlling porosity and permeability. Although much work has already been done on describing and interpreting specific diagenetic processes and diagenetic environments (e.g., Wilson, 1975; Longman, 1980; Harris et al., 1985; Tucker and Wright, 1990; Tucker, 1993; Moore, 2001), the interpretation and prediction of porosity evolution in carbonate rocks remains difficult (e.g., James and Choquette, 1990; Dix and Mullins, 1992; Frank and Bernet, 2000). A wide variability in porosity evolution exists throughout sedimentary facies and under different geological circumstances. Moreover, reservoir porosity is the result of a complex interplay of geological processes (e.g., Saller et al., 1994; Hendry et al., 1999; Whitaker et al., 1999). Therefore, good case studies of porosity evolution are required to deduce controlling factors and to predict reservoir characteristics through time (e.g., Feazel and Schatzinger, 1985; Minero, 1991; Sun et al., 1992; Saller et al., 1994; AlAasm and Azmy, 1996; Aqrawi et al., 1998; Ehrenberg et al., 1998; Madi et al., 2000; Budd, 2001; Saller et al., 2001). In this respect, outcrop analogues are of special importance, since porosity variations can be studied in three or even four dimensions (space and paragenetic evolution = time).

The Cordoba Platform limestones in eastern Mexico underwent complex diagenesis, reflecting a long history of fluid circulation since deposition, through Laramide foreland evolution and deformation and still continuing, leading to reservoir preservation/development and an oil-migration and -trapping history (Ortuño-Arzate et al., 2003). Most reservoirs in the studied area are fracture controlled. Some, however, display matrix porosity and a lithologic control of hydrocarbon occurrence. For this study, the Peñuela quarry was selected, since alternating nonimpregnated and (residual) oil-impregnated strata are exposed here.

The main object of this study is to illustrate the diagenetic and, especially, the porosity evolution of the Peñuela area by petrographic and isotopic investigation and to reveal the controlling mechanisms responsible for matrix-porosity preservation and development. Therefore, the porosity evolution will be fitted on the structural evolution based on forward kinematic modeling (Ortuño-Arzate et al., 2003). This study is of importance since, based on core observations (e.g., M.R. Aguilar 1A Well cores), some of these

diagenetic processes also may have affected the oil reservoirs occurring in the subsurface of the nearby Veracruz Basin.

GEOLOGICAL SETTING

The Peñuela quarry (Plate 1A) is situated east of the city of Cordoba in the western part of the state of Veracruz (eastern Mexico, Figure 1). The outcrop is part of the Cretaceous Cordoba carbonate platform that forms a lithological and structural entity between the western Zongolica Basin and the eastern Veracruz Basin (Ortuño-Arzate et al., 2003). Structurally, the Cordoba Platform belongs to the foreland fold and thrust belt of the Laramide orogeny. A large décollement surface follows the Lower Cretaceous evaporitic layers (Figure 2; Ortuño-Arzate et al., 2003). The Laramide orogeny started at the end of the Cretaceous. During the Paleocene, the deformation prograded through the foreland, and flysch sediments were deposited over the platform and in the eastern Veracruz Basin. After Laramide orogeny, sedimentation was restricted to the Veracruz Basin, and the platform to the west was exposed to erosion. At present, thrust sheets with large ramp anticlines crop out to the west but are buried to the east beneath the Veracruz Basin, where they end in a stack of duplex structures.

Kinematic modeling (Ortuño-Arzate et al., 2003) demonstrated that temperatures in the western part of the platform remained below 50°C during the burial-deformation history of the foreland. Foreland burial was limited (probably <2.5 km). The thin-skinned thrust sheets always remained in a superficial position, and after Laramide deformation, they remained elevated. Only in the buried tectonic front were temperatures sufficient to reach the oil window. There are a number of large oil fields (e.g., Mata Pionche, Copite, Mecayucan) in this tectonic front zone.

Upper Cretaceous strata of the Guzmantla Formation crop out in the studied quarry. The Guzmantla Formation consists of a lower Turonian part with deposition in an outer platform environment and an upper Coniacian to Santonian part reflecting an inner platform with isolated lagoons (Figure 3). The outcropping strata in Peñuela are most probably of early Coniacian age, since they constitute the lower part of the formation but already reflect inner-platform conditions. Time-equivalent strata with a dual matrix/fracture porosity are producing in wells to the east in the buried Laramide thrust front.

METHODOLOGY

The description of diagenetic phenomena and the deduction of the paragenetic sequence are based on petrographic examination (polarizing microscope, cathodoluminescence [CL], and scanning electron microscope [SEM]) of 65 thin sections of representative carbonate rocks. Cathodoluminescence was performed on a cold Cathodoluminescence Technosyn Model 8200 MkII, by 620 μA current and between 16 to 20 kV. Electron microscopy was performed on gold-coated samples using a JEOL-JSM 6400. Operating conditions were 15 kV, 60 μA, and about 600Å beam width.

Crosscutting relationships between the cement phases and the different stylolite generations (compactional and tectonic; Andrews and Railsback, 1997) allow a relative dating of the diagenetic phases. Bed-parallel stylolites (BPS) and dissolution seams are formed parallel to bedding as a result of chemical compaction by pressure solution under long-term stress (Logan and Semeniuk, 1976; Meyers, 1980; Railsback, 1993; Bathurst, 1995). Layer-parallel shortening stylolites (LPSS) are caused by tectonic shortening and form stylolitic planes perpendicular to bedding (Whitaker and Bartholomew, 1999). The recognition of these two stylolite sets enables linkage of diagenetic evolution with the deformation history of the area.

In order to determine the fluid characteristics, various cement phases and bulk lithologies were sampled for stable isotopical analyses. A dentral drill was used to collect carbonate samples (at least 2 mg) for oxygen and carbon isotope analyses. Carbonate powders were reacted with 100% phosphoric acid (density > 1.9, Wachter and Hayes, 1985) at 25°C in an online carbonate preparation line (Carbo-Kiel—single-sample acid bath) connected to a Finnigan Mat 252 mass spectrometer. All values are reported in per mil relative to V-PDB (‰VPDB) by assigning a $\delta^{13}C$ value of +1.95‰ and a $\delta^{18}O$ value of −2.20‰ to NBS19. Reproducibility was checked by replicate analyses of laboratory standards and is better than 0.02‰ and 0.04‰ (±1σ), respectively. The original signature of marine Cretaceous carbonates is accepted to vary between −2.5 and −1‰ VPDB for oxygen and between +2 and +3.5‰VPDB for carbon, based on reported values of Czerniakowski

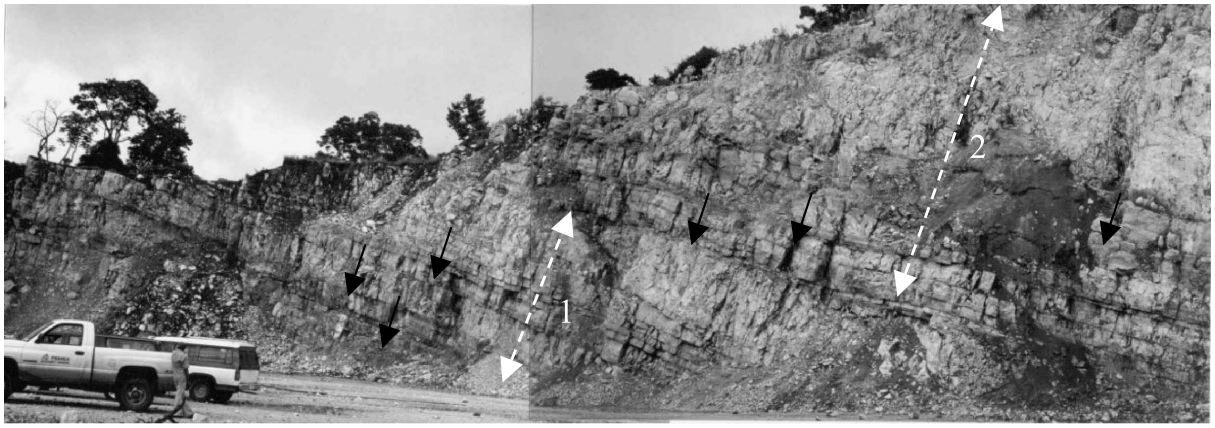

A

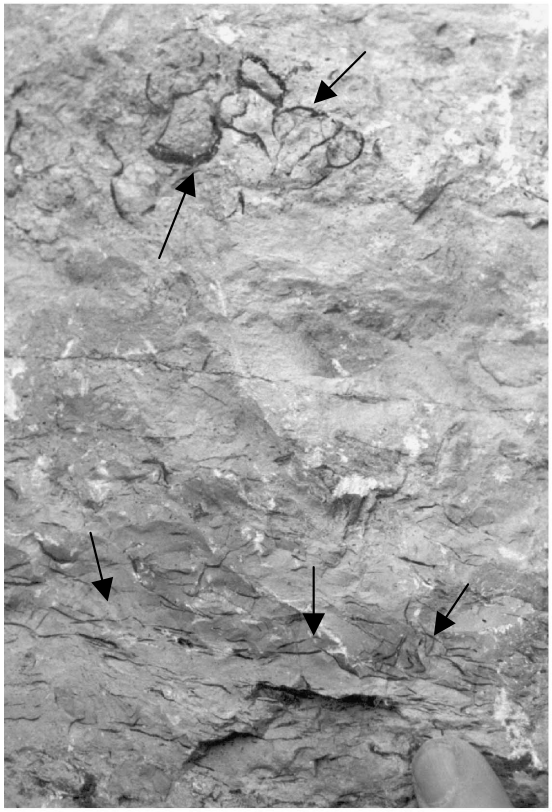

B

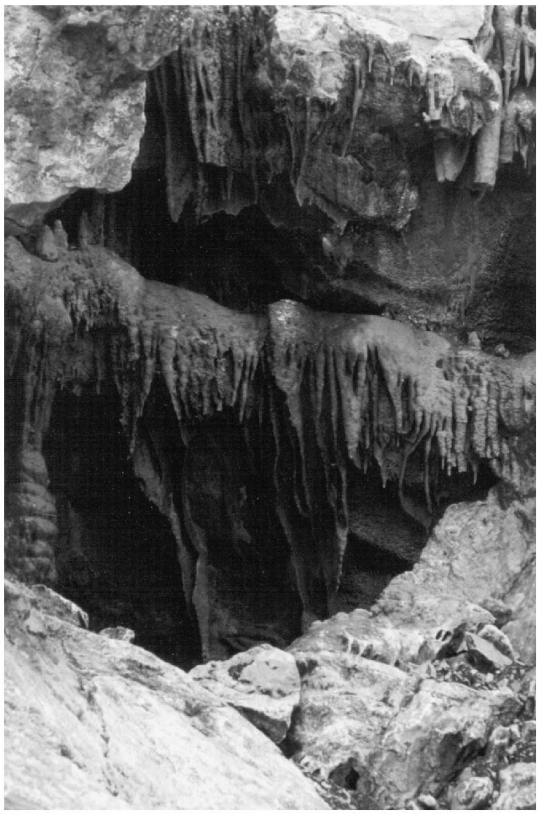

C

D

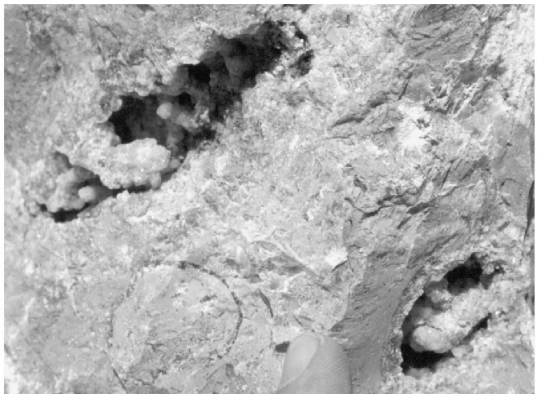

E

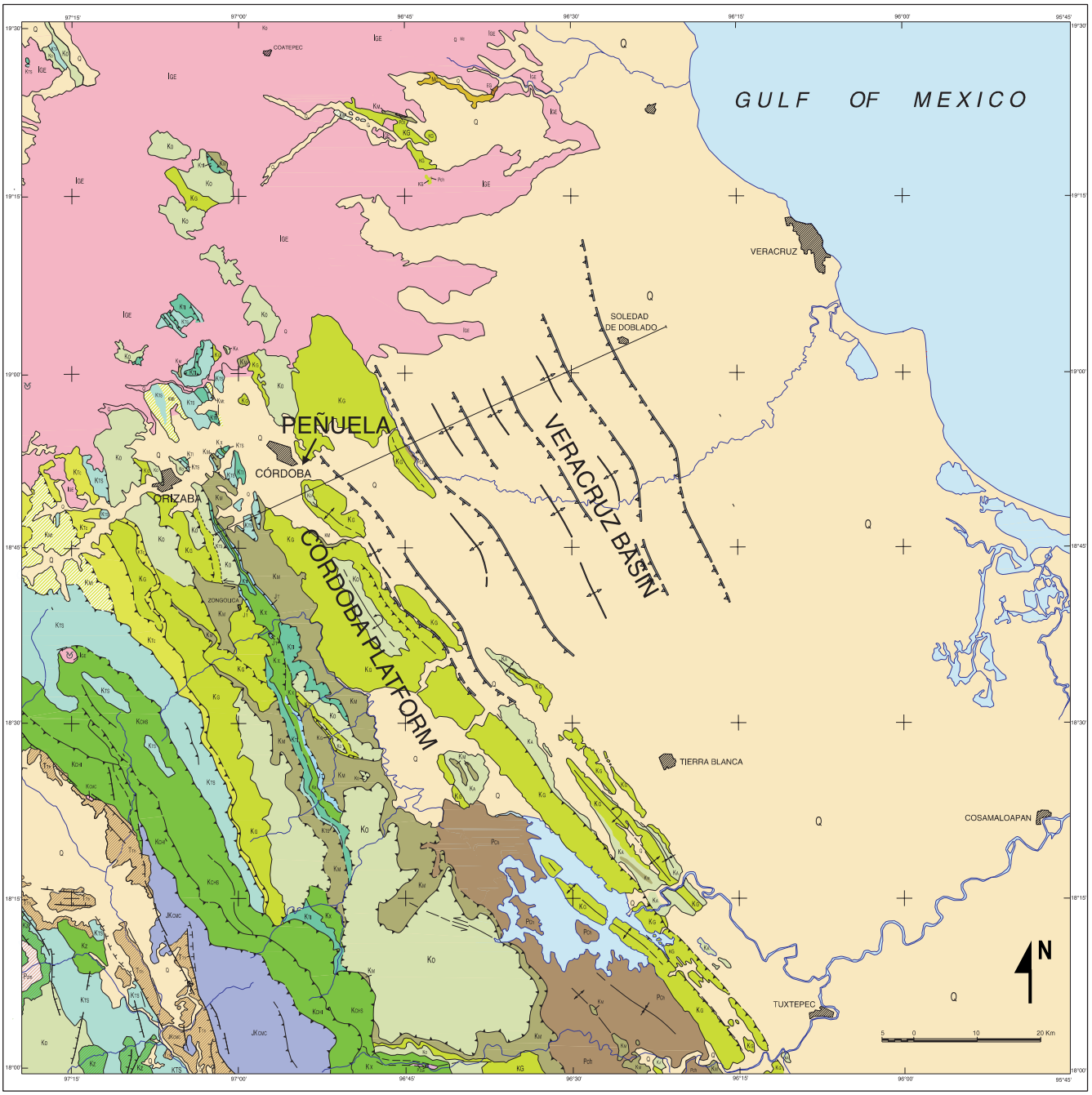

Figure 1. Geological map of the Laramide foreland fold and thrust belt in the Cordoba Platform–Veracruz Basin area. Note the location of the structural cross section of Figure 2, along which a Thrustpack kinematic modeling has been carried out (Ortuño-Arzate et al., 2003).

et al. (1984) for Coniacian-Santonian carbonates and the values of Swennen and Dusar (1996) and Frank and Arthur (1999) for Campanian-Maastrichtian carbonates.

OUTCROP FEATURES

The Guzmantla limestones, which crop out in the Peñuela quarry, form a succession of well-bedded,

Plate 1. Outcrop features in the Peñuela quarry. (A) Selectively oil-impregnated strata (indicated with black arrows) in the Peñuela quarry. Numbers 1 and 2 indicate the two coarsening upward cycles. (B) Oil-impregnated biomolds (arrows) in Lithotype II. (C) Cavern porosity with speleothem cementation. (D) Pervasively impregnated Lithotype II strata. Note that oil is also present along joint planes (arrow). (E) Nonoil-stained telogenetic biomoldic and vuggy dissolution in Lithotype III strata.

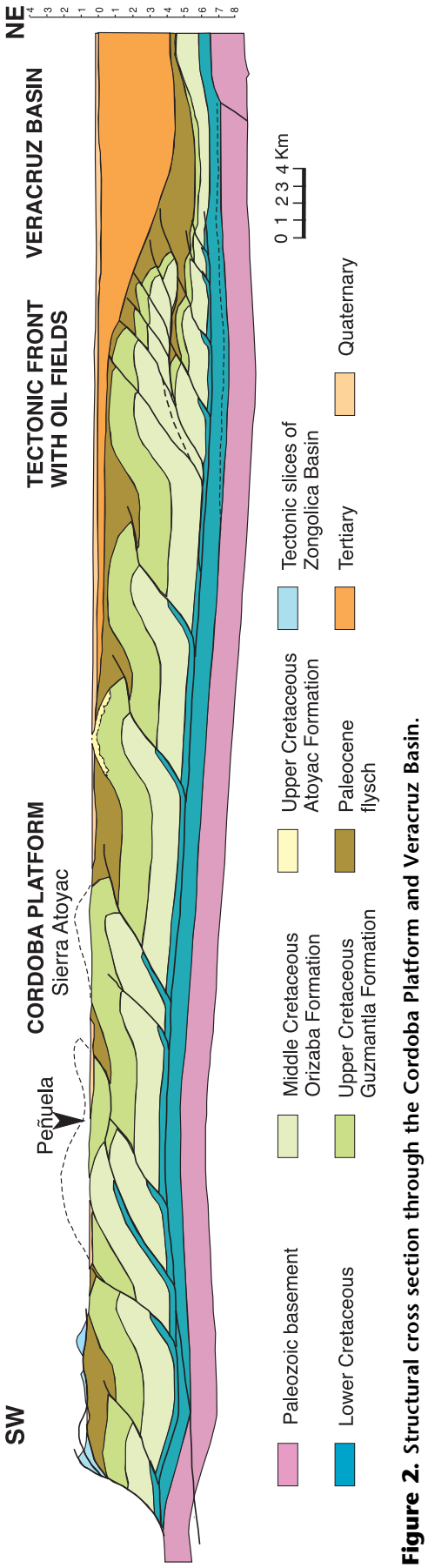

Figure 2. Structural cross section through the Cordoba Platform and Veracruz Basin.

gently dipping strata. At least two superimposed 20-m-scale upward-coarsening cycles (Figure 4) culminating in thick-bedded (6–10 m) coarse-grained bioclastic grainstone strata can be distinguished (Plate 1A). The vertical succession through one cycle is comprised of a basal part, starting with thin (0.1–0.5 m), dark-colored shaly beds and (laminated) mudstones with abundant oil-stained dissolution seams. Subsequently, a dark-colored fine-grained part (2–4 m in thickness) is comprised of mudstones to wackestones. These strata are characterized by the presence of numerous oil-stained dissolution seams and stylolites and dispersed oil-filled biomolds occurring next to stylolitic planes. These strata grade upward into bioclastic and peloid-rich wackestones to packstones that are alternately pervasively oil-impregnated and non- or slightly oil-impregnated. Extensively burrowed and some shell-debris horizons occur in this section. This debris consists mostly of rudist shells, which are cemented or have been (partly) dissolved and subsequently filled with oil. Oil-stained stylolites are omnipresent. The upper part of the cycle consists of a thick-bedded (6–10 m), light-colored, coarse-grained bioclastic grainstone interval, but despite the fact that it displays macroporosity (mostly biomoldic), it lacks oil-impregnation. In these strata, stylolites are also virtually absent.

A highly viscous (residual) oil is present in the lower and middle parts of the sedimentary cycles, i.e., as interparticular pore filling, in large biomolds (Plate IB), in both bed-parallel (BPS) and perpendicular (LPSS) stylolite planes (Plate 2A), in open joints (Plate 1D), and in some of the open fractures (Plate 2B).

Many recent karst features are present in this quarry, varying from small-scale dissolution traces to cavern porosity with speleothem development (Plate 1C). Large open biomolds and vugs occur (Plate 1E), which have not been filled with oil and which have been filled partially with mm-sized euhedral calcite cements.

PETROGRAPHY

Sedimentary Characteristics

Based on the oil staining (Figure 4) and sedimentological and diagenetic characteristics, three main lithotypes can be distinguished. Although the lithotypes can group several different lithofacies, this division is used to simplify the description of the diagenesis and porosity evolution.

Lithotype I (Plate 2B, D, and E) consists of highly compacted, poorly cemented, mud-dominated lithologies

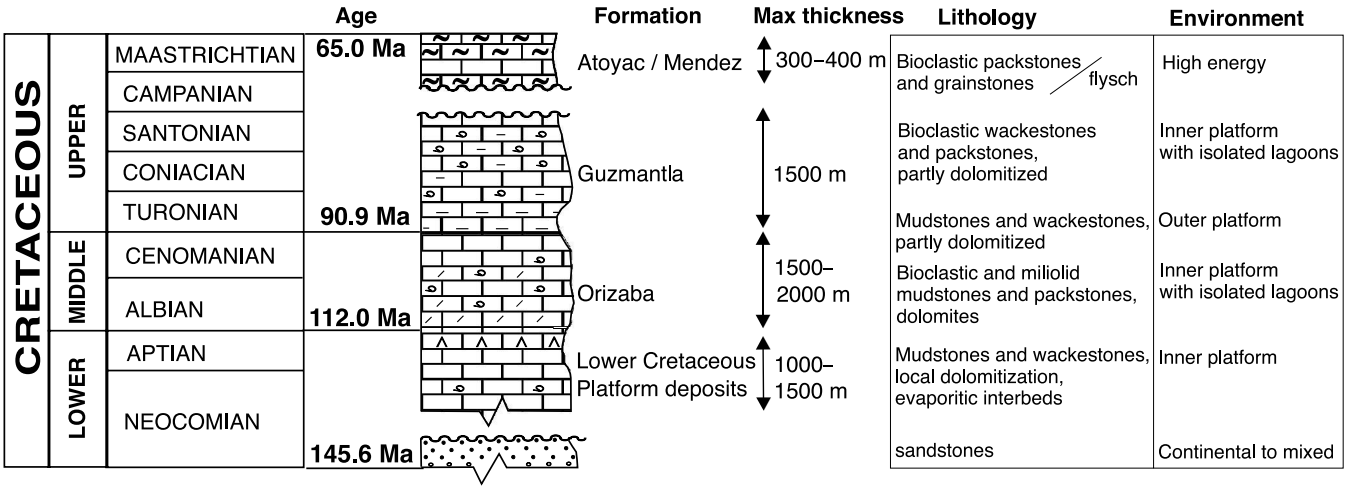

Figure 3. Stratigraphic log of the Cretaceous deposits in the Cordoba Platform.

with oil staining restricted to dissolution seams and stylolites. This lithotype builds up mainly the basal part of the sedimentary cycles and some more compacted and mud-dominated facies of the middle part. It is comprised of thin shaly interbeds and (laminated) mudstones with ostracods, foraminifera, and pellets, pointing out a low-energy environment. Also, peloidal to foraminiferal wackestones and bioclastic wackestones with rudists, gastropods, and foraminifera in a micrite matrix are classified in Lithotype I and

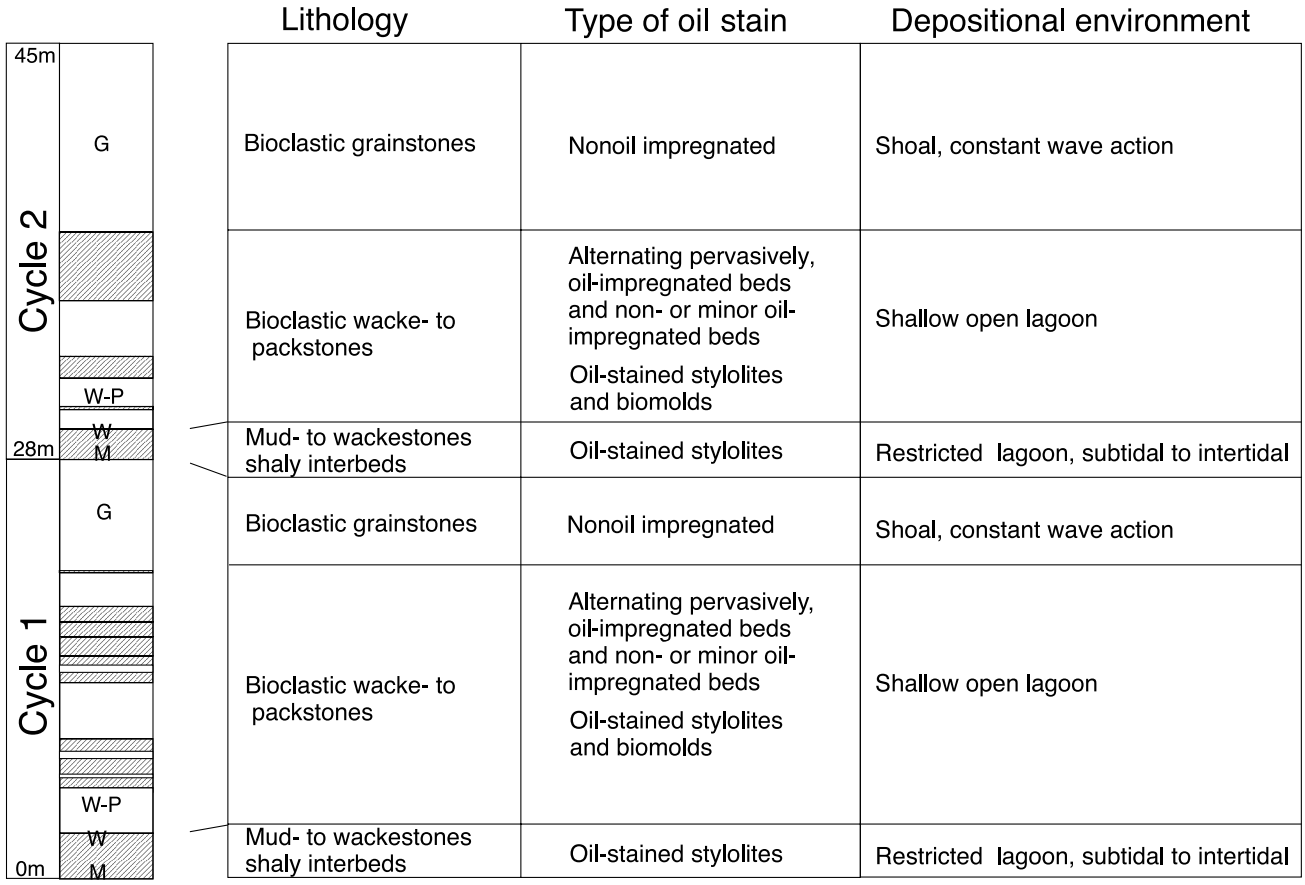

Figure 4. Measured section of the Peñuela outcrop. Shaded areas indicate oil impregnation. G = grainstones, W-P = wackestones to packestones, W = wackestones, M = mudstones.

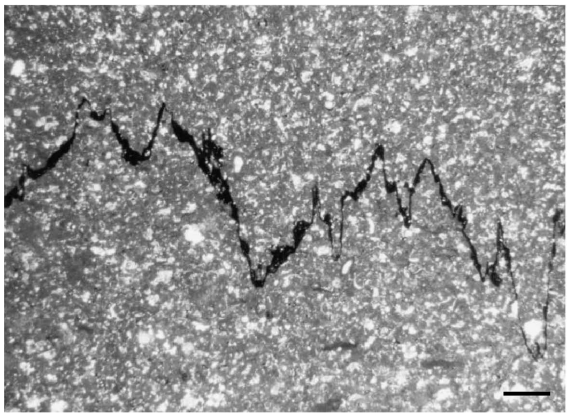
A


B

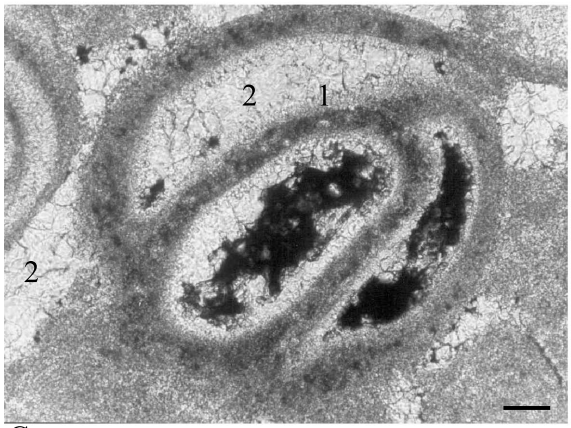

C

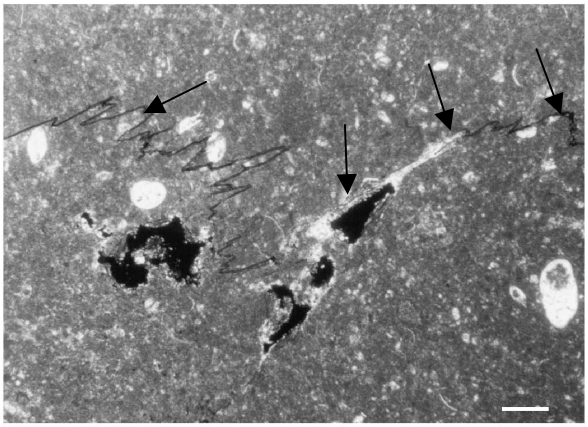
D

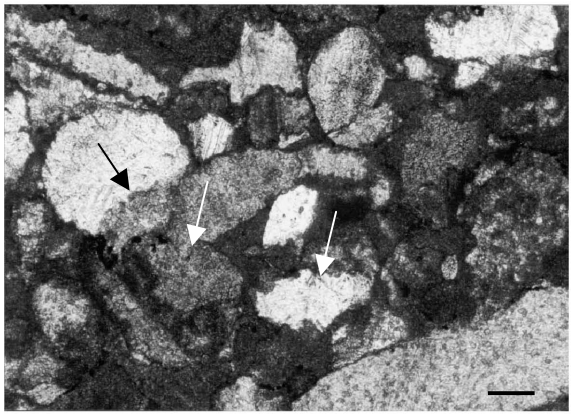
E

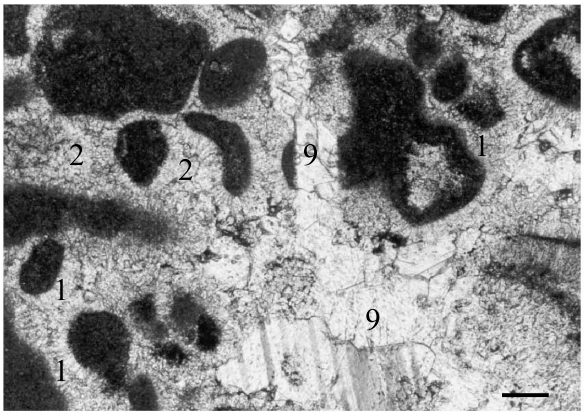

F

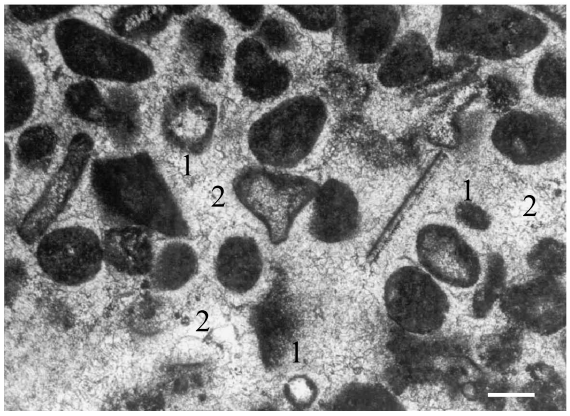

G

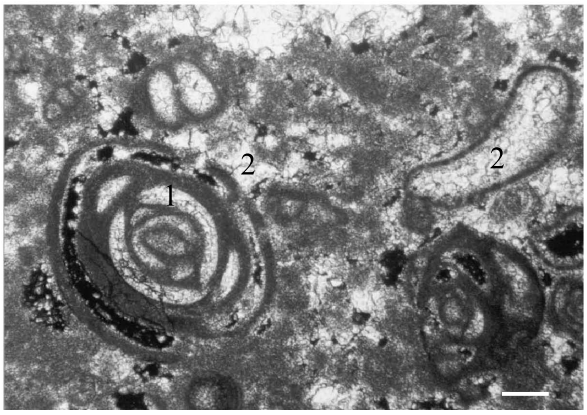

H

are typical of low-energy subtidal or intertidal restricted conditions. Furthermore, stromatolitic facies occurs, grading sometimes upward into pelsparites with thin mud intercalations, as well as fenestral fabric; they are most common in the intertidal zone. Stylobrecciated wackestones to packstones are present as thin intercalations in mudstones and wackestones or as thicker strata. They are characterized by debris accumulation of crystalline fragments of rudists, crinoids, and foraminifera, next to pellets and completely micritized bioclasts and lithoclasts. These debris layers are interpreted as lag deposits in intertidal channels. Closely spaced bed-parallel dissolution seams and stylolites as well as LPS-stylolites occur in Lithotype I strata. Oil impregnation in these strata is restricted to the dissolution seams, stylolites (Plate 2A), and to biomolds close to oil-stained stylolites (Plate 2D).

Lithotype II (Plate 2A, C, and H) groups pervasively oil-impregnated bioclastic wackestones to packstones of the middle part of the cycles. Compared to the basal part, a general coarsening-upward trend is developed in the middle part of the cycles, although some intercalations of finer, low-energy facies (Lithotype I) still occur. Bioclastic wackestones to packstones contain a variety of coated or sometimes micritized bioclasts, such as rudists, echinoderms, foraminifera, gastropods, algae, and sponges, as well as peloids. Rudist shell-hash wackestones and packstones with a coating of algal filaments around the shells are common. These deposits are typical of a shallow, open-lagoonal environment, close to rudist buildups. Numerous BPS as well as LPS-stylolites developed in these strata.

Lithotype III (Plate 2F and G) makes up the upper part of the cycles. It corresponds to nonoil-impregnated, bioclastic grainstones containing fragments of rudists, gastropods, foraminifera, echinoderms, and peloidal lithoclasts (micritized and rounded fragments). Particles are generally well rounded, well sorted, and coated with a micrite rim or completely micritized. Lime mud has been removed, and the grains float in a sparite matrix. These strata are typical of a shoal, where constant wave action removes the lime mud and makes the particles sorted and rounded. Sometimes, thin intercalations (in one thin section) of mudstones and wackestones occur, pointing out a more restricted environment with lower energy. These intercalations can be related to tidal variation of water energy.

Diagenetic Features and Paragenesis

The three lithotypes display different diagenetic features. Lithotype I is strongly compacted and lacks significant cementation; consequently, it is characterized by low matrix porosity. Porosity occurs only along stylolites and is oil-impregnated. Lithotype II has undergone compaction but also contains inter- and intraparticular calcite cement. Modern porosity is high (5–15%, visual estimate) and consists of inter- and intraparticular as well as biomoldic pores. Lithotype III's primary porosity is almost entirely cemented by an isopachous acicular calcite cement and subsequent equant calcite cement and shows virtually no apparent compaction phenomena. Paleoporosity is limited to less than 0.5%, except for some large bioclasts in which primary intraparticular porosity is preserved, raising paleoporosity locally to about 5%. However, as described below, Lithotype III strata became selectively strongly affected by telogenetic karst development. The large secondary biomolds and vugs account for an increase in porosity, raising the modern porosity to about 15% to 20%.

Based on the development of compactional bed-parallel stylolites (BPS) as well as tectonic layer-parallel shortening stylolites (LPSS), the diagenetic history (Figure 5) can be split into three major episodes, as described below.

Pre- to Syn-BPS Diagenesis

The pre- to syn-BPS diagenetic evolution is dominated by two dissolution phases, a fracturing phase, the precipitation of four types of calcite cements, and physical and chemical compaction of the strata.

Plate 2. **Petrographic features of the Guzmantla lithologies in the Peñuela quarry. (A) Oil-impregnated stylolite in Lithotype II. Scale = 625 μm; (B) Crack-and-seal fracture with white calcite cement and oil (dark spots) in mudstone (Lithotype I). Scale = 625 μm; (C) Calcite 1 (1) and 2 (2) cement filling inter- and intraparticle pore space in Lithotype II. Scale = 50 μm; (D) Oil-stained stylolite (traced by arrows and partially accentuated) and oil-impregnated enlarged biomolds next to this stylolite. Scale = 310 μm; (E) Strongly compacted wackestone to packstone (Lithotype I). The arrows indicate sutured grain boundaries. Scale = 100 μm; (F) Calcite 9 cement cross-cutting the early formed Calcite 1 and 2 cements in bioclastic grainstone (Lithotype III). Scale = 100 μm; (G) Abundant early-marine (Calcite 1) and meteoric (Calcite 2) cementation in bioclastic grainstone (Lithotype III). Scale = 100 μm; (H) Bioclastic wackestone to packstone (Lithotype II) with Calcite 1 and 2 cement and oil-filled inter- and intraparticular porosity (black spots). Scale = 100 μm.**

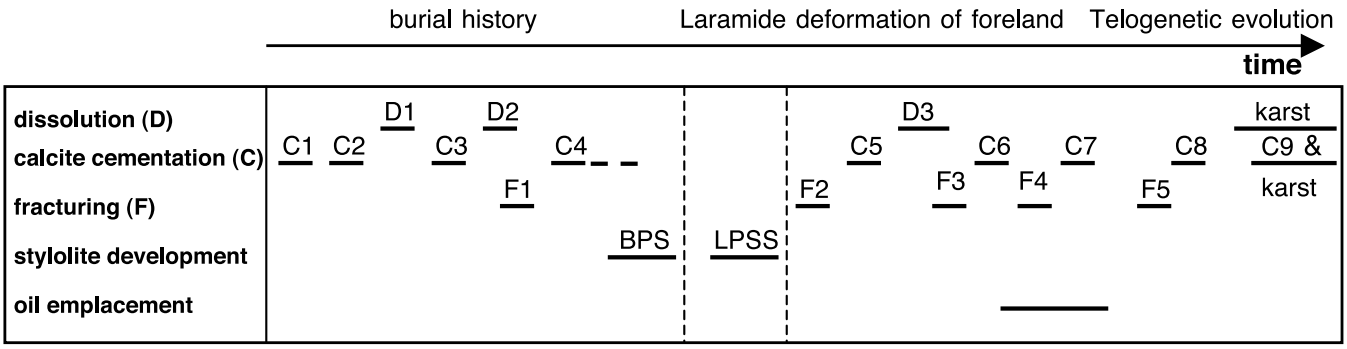

Figure 5. Paragenetic sequence of the Guzmantla Formation strata outcropping in the Peñuela quarry.

Four calcite cement types predating BPS development have been identified, namely (1) a nonluminescent acicular isopachous cement (Calcite 1), (2) a nonluminescent equant cement (Calcite 2), (3) a zoned luminescent columnar to equant cement (Calcite 3), and (4) a dull luminescent, slightly sector-zoned equant cement (Calcite 4). Calcite 3 follows the development of biomolds and vugs (dissolution phase 1, D1). A minor dissolution (D2) and fracturing phase (F1) affected Cement 3 and are followed by Calcite 4 cementation (Figure 5).

The nonluminescent acicular isopachous calcite cement (Calcite 1) surrounds inter- and intraparticle pore spaces in Lithotype III (Plate 2F and G). These acicular to columnar crystals are about 10 to 50 μm long and form a massive 3-D network, as observed by SEM (Plate 4A). They constitute about 20% of the bulk rock volume (B.V.). In Lithotype II, this type of cement is less developed (about 5 to 10% B.V.). Here, it is characterized by 5–15 μm long acicular crystals lining inter- and intraparticular pore spaces (Plates 2C, 4C, and 4D). Lithotype I lacks Calcite 1 cement development.

The nonluminescent equant cement (Calcite 2) has a drusy texture and fills most of the remaining primary pore space in the acicular calcite-cemented grainstones of Lithotype III (Plate 2F and G); it precipitated as an inter- and intragranular cement in the bioclastic wackestones of Lithotype II (Plates 2C, 2H, 4C, and D). The occurrence of this cement is rare in Lithotype I.

Biomolds, preferentially affecting gastropods and rudists, and small vugs developed in Lithotype II and III during dissolution phase 1. A non-yellow to bright-yellow and dull-yellow finely zoned equant to columnar calcite cement (Calcite 3, Plate 3D), ranging in size between 5–25 μm or even as much as more than 500 μm occurs in primary intra- and interparticle pores and secondary biomoldic and vuggy pores created by dissolution phase 1. Calcite 3 also occurs as an overgrowth cement (Plate 3E), forming an irregular rim around shell fragments (echinoderms, rudists, gastropods) in mud-rich lithologies in Lithotypes I and II. Calcite 3 cement is locally fractured and affected by dissolution (dissolution phase 2). In the shell-hash facies of Lithotype II, rudist shells overgrown by Calcite 3 have been broken by mechanical compaction and subsequently have been cemented by a dull to nonluminescent equant calcite cement (Calcite 4). Calcite 4 precipitated into the remaining primary and secondary pores (Plate 3D and E), as well as in fractures cutting through Calcite 1 to 3.

The total cement volume in Lithotype III comprises about 30 to 40% B.V., in Lithotype II, about 15 to 20% B.V., whereas Lithotype I lacks significant cementation (<5%). The fact that primary interparticular porosity still exists in Lithotype II points toward framework-stabilizing cementation (Plate 4D) that, however, did not occlude completely the porosity as in Lithotype III. It means that the interparticular cements were distributed in a way to form a rigid structure capable of resisting strong compaction of the matrix but not occluding the porosity. The remaining interconnected pores, consequently, also formed potential sites for later fluid flow by which porosity can be further enhanced or reduced.

Physical compaction is manifested in Lithotype I and, to a lesser degree, in Lithotype II, by fracturing of shells, deformed particles, and grain contacts (Plate 2E). Chemical compaction as a result of pressure dissolution resulted in the development of sutured grain boundaries (in bioclastic-rich facies, Plate 2E), dissolution seams (in muddy and clay-rich facies), and stylolite development (Plate 2A). Fractured particles and cements were healed by cements, especially by Calcite 4. It is likely that the dull luminescent Calcite 4 cement also was precipitated during

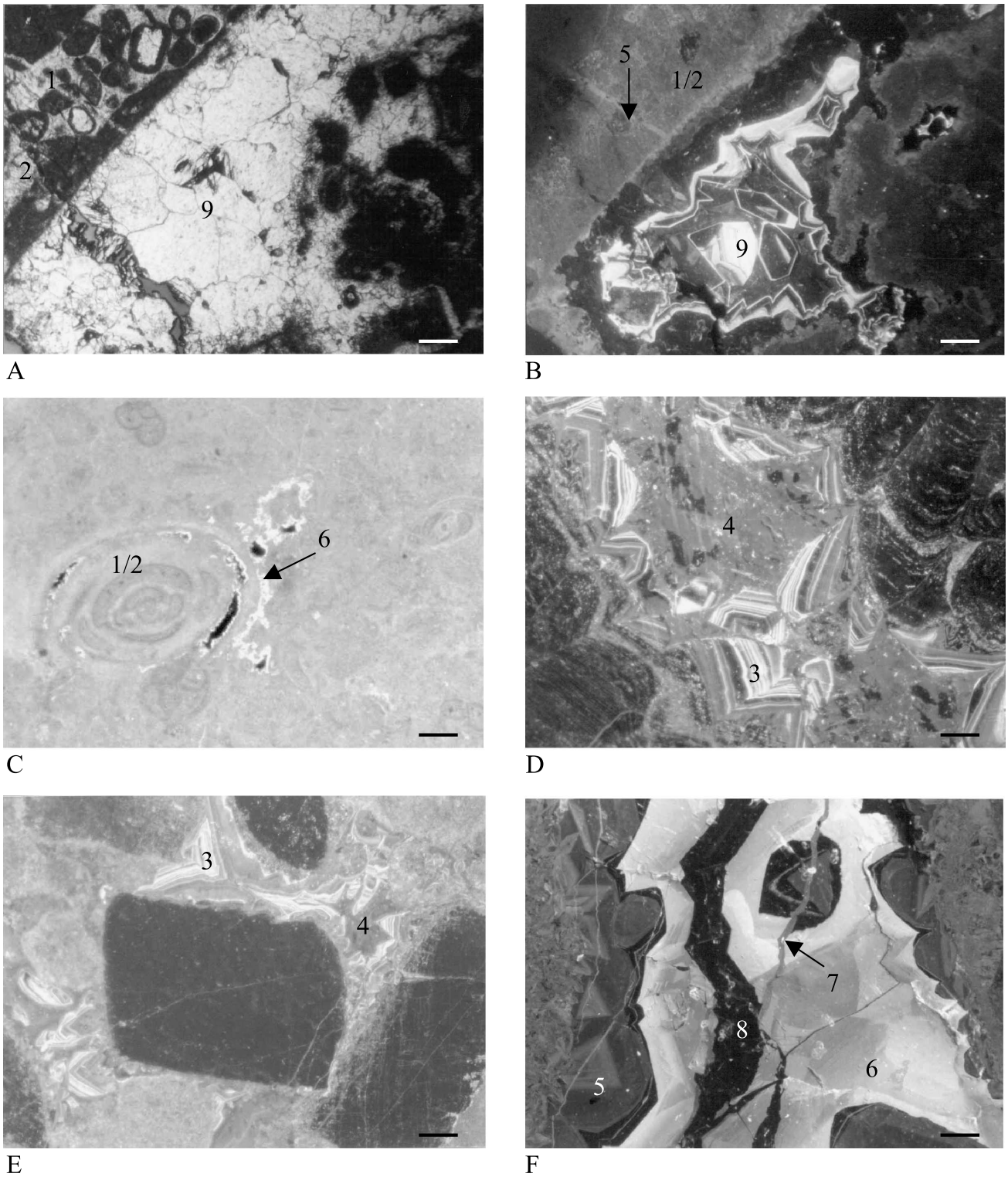

Plate 3. Cathodoluminescence (CL) patterns. (A) Transmitting light view of Plate 3B with vug filled with Calcite 9 cement in a bioclastic grainstone with Calcite 1 and 2 cement. Scale = 100 μm; (B) CL image of Plate 3A, vug filled with nonluminescent, bright-yellow-luminescent , and dull-brown-luminescent zoned Calcite 9 cement in a bioclastic grainstone cemented with non-luminescent Calcite 1 and 2. Note the small fracture filled with dull-luminescent Calcite 5 cement. Scale = 100 μm; (C) Bright-yellow luminescent Calcite 6 cement in inter- and intraparticular pores in a nonluminescent wackestone (Lithotype II). Note that oil (black color) is present in these pores. Scale = 100 μm; (D) Nonluminescent and bright-yellow luminescent zoned Calcite 3 and dull luminescent Calcite 4 cement. Note that the Calcite 3 crystals have been corroded before precipitation of Calcite 4. Scale = 100 μm; (E) Calcite 3 as overgrowth cement around grains and Calcite 4 occluding the remaining porosity. Scale = 100 μm; (F) Post-LPSS fracture composed of several cement subgenerations filled successively with Calcite 5, 6, 7, and 8. Scale = 100 μm.

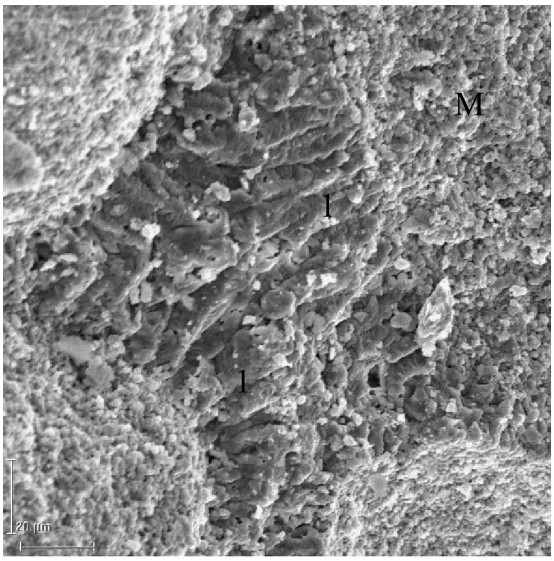

A

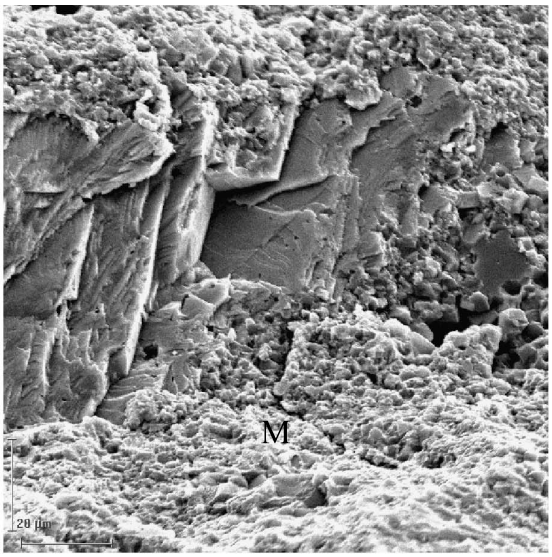

B

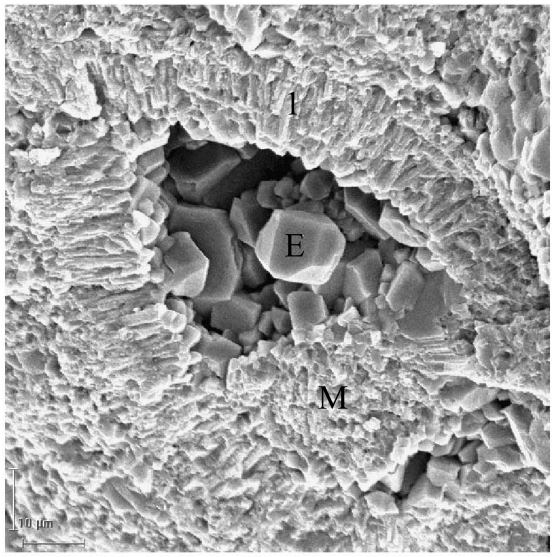

C

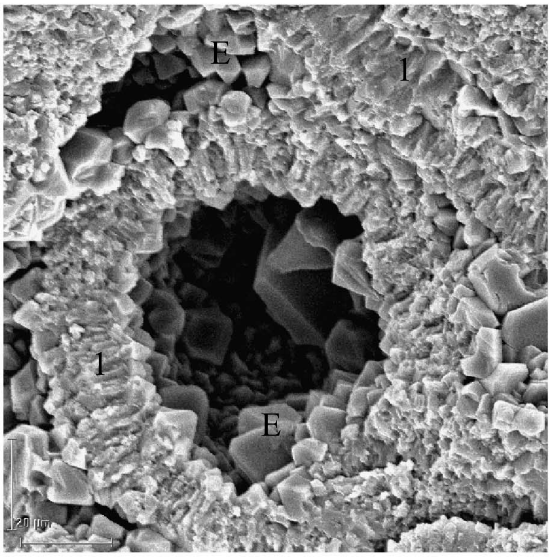

D

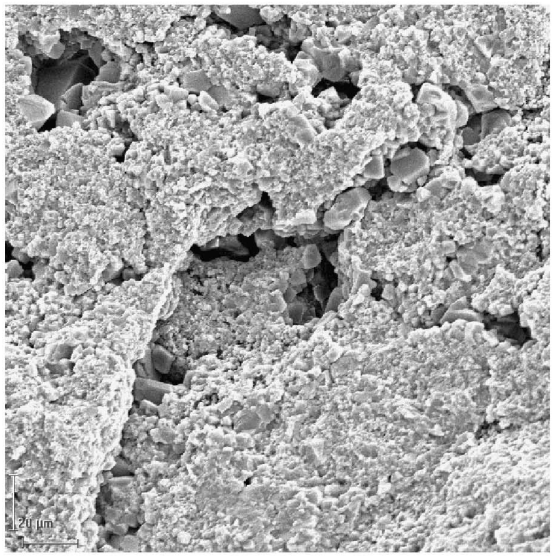

E

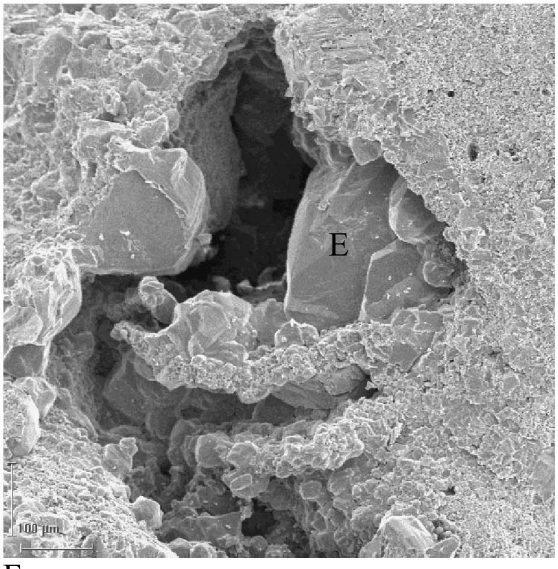

F

BPS development, since compaction of fine-grained facies generates a flux of $CaCO_3$-rich fluids that precipitate in open pores (Matter, 1974; Morse and Mackenzie, 1993; Heydari, 2000). Since compaction stylolites (BPS) are believed to form at burial depths starting from 800–1500 m (Railsback, 1993) or even less, depending on the lithology, the time period of BPS development can be constrained to around the beginning of the Paleocene, which agrees with kinematic modeling (Ortuño-Arzate et al., 2003).

Post-BPS/Pre- to Syn-LPSS Diagenesis

Although cemented fractures (mainly hydraulic fractures) that postdate BPS and predate LPSS are common in other studied outcrops of the Cordoba Platform, these fracture generations have not been identified in the Peñuela outcrop. This is not to say that these phases do not occur. Some fractures lack crosscutting relationships with one of the stylolite sets so that they cannot be placed exactly (in relation to both BPS and LPSS) in the paragenetic sequence. From the study of cemented fractures in several outcrops throughout the Cordoba Platform, some general trends were deduced. Post-BPS cemented fractures show a trend toward higher temperatures (deduced from stable isotopes and the presence of saddle dolomite). The highest temperatures are reached just before and during the layer-parallel shortening stage, while later post-LPSS phases point again toward lower temperatures and the latest phases toward karst development (Ferket et al., 2000; Ortuño-Arzate et al., 2003, and unpublished data). Due to the increasing horizontal (tectonic) stress, fluids are expelled and layer-parallel shortening structures develop.

The stylolite set perpendicular to stratification, caused by layer-parallel shortening, is characterized generally by relatively higher-amplitude stylolite planes. They crosscut BPS planes and Calcite 1 to 4 cements. They are believed to develop immediately prior to folding and thrusting of the strata (Averbuch et al., 1992; Mitra, 1994; Railsback and Andrews, 1995; Storti et al., 1997; Tavarnelli, 1997; Storti and Salvini, 2001). Based on the kinematic modeling (Ortuño-Arzate et al., 2003), the timing of this LPS deformation can be constrained to the Paleocene. This implies that the period of time between BPS and LPSS development was relatively short.

Post-LPSS Diagenesis

Post-LPSS carbonate dissolution (D3, Figure 5) took place along stylolites, leading locally to permeability paths with a pore width on the order of 100–200 μm. Stylolites form initially impermeable structures because of the concentration of insoluble material along their planes. Since many stylolites are oil-impregnated and some have been filled in with calcite cement, they must have been opened and used by fluids following these heterogeneities. Remarkably, oil impregnation in matrix porosity is favored adjacent to stylolitic planes. Oil-filled biomoldic to vuggy porosity that is related to a third dissolution phase (D3) occurs along stylolites (Plate 2D) in Lithotypes I and II. In the permeable Lithotype II strata, this dissolution also generated enlarged inter- and intraparticular pores, as well as biomolds.

Additionally, different post-LPSS calcite cement generations have been distinguished based on their cathodoluminescence characteristics and crosscutting relationships. A dull-luminescent calcite cement (Calcite 5) displaying a slight sector zonation pattern or forming zoned euhedral calcite crystals filled an early post-LPSS fracture generation. Subsequently, a bright-yellow luminescent-zoned calcite cement (Calcite 6) precipitated in the remaining fracture pores or in newly formed open fractures. This bright-yellow luminescent calcite cement also often occurs along stylolites and as a cement rim in biomolds and interas well as intraparticle pores (Plate 3C). Locally, in strongly stylolitized facies, the micrite matrix has been altered, i.e., recrystallized into bright-yellow luminescent calcite. Fractures cemented with a dull-luminescent calcite cement (Calcite 7) cut through the earlier cemented fractures. This cement phase was cut by a later fracture generation filled with a non-luminescent calcite cement (Calcite 8, Plate 3F).

Oil occurs along stylolites (Plate 2A and D), in inter- and intraparticle pore spaces (Plates 2C, 2H,

Plate 4. SEM-images. (A) Acicular isopachous Calcite 1 cement in Lithotype III. M indicates the micritized rim around the particles; (B) Mudstone with compacted micrite (M) and bioclast; (C) Calcite 1 cement in a foraminifer with micrite rim (M). Equant cements (E; probably Calcite 2) partly fill the intraparticle pore space; (D) Framework-stabilizing cementation by early Calcite 1 and 2 cement in oil-impregnated Lithotype II matrix (oil was removed prior to scanning). Appreciable inter- and intraparticle porosity is still open. E = pre- or post-LPSS equant cement; (E) 3-D pore network in oil-impregnated Lithotype II matrix; (F) Biomold partly filled with equant cement (E; possibly Calcite 9) in Lithotype III.

4C, 4D, and 4E), in biomolds and small vugs (Plate 2D), and in some fractures cemented by the bright-yellow-zoned (Calcite 6) and by dull-luminescent-zoned (Calcite 7) cements (Plate 2B). Oil emplacement thus took place after these cements filled the fractures.

A non- to bright-yellow- to dull-luminescent-zoned equant calcite cement with crystal faces in the order of 50–500 μm (henceforth called Calcite 9, Plate 1E) occurs in dissolution vugs and biomolds in Lithotype III, thereby cutting through earlier precipitated pre-BPS cements (Plate 2F, 3A, and 3B). Even when these pores are not completely filled with Calcite 9, oil is absent from the pores. Fractures cutting through the oil-filled structures in Lithotype II also are filled with this bright-yellow- luminescent-zoned Calcite 9 cement. Consequently, they are interpreted to postdate oil migration.

Other macroscopic dissolution features observed in the quarry are channel porosity at different scales (from a few centimeters to several meters) that is often filled with an internal sediment (i.e., terra rossa). Small or larger (centimeter scale) vugs are bordered by an euhedral calcite cement. Cavern porosity is partly filled with speleothem cementation (e.g., stalactites and calcite rosettes). These dissolution features and cements, as well as several calcite cement generations along open-joint planes and in open fractures, point toward the importance of a telogenetic karst development (Plate 1C). The late-stage (recent) karst-related cements are all characterized by their nonluminescent aspect, but they are not described further in detail here. As they postdate oil migration, splitting them up into different subgenerations of calcite provides no essential information for our study. Noteworthy is that Lithotypes I and II are clearly less affected by this major telogenetic dissolution phase than Lithotype III.

STABLE ISOTOPES

The stable isotope analysis results are given in Figure 6, together with the marine signature for Middle to Upper Cretaceous carbonates.

Bulk matrix analyses of mudstones (Lithotype I), wackestones (Lithotype II), and grainstones (Lithotype III), whereby mainly bioclasts, micrite, and Calcite 1 and 2 cements have been sampled, plot together, mainly in one cluster. Two samples of rudist shells, which have been overgrown mainly by Calcite 3, as well as Calcite 3 and 4–cemented gastropod and rudist biomolds, plot within the same cluster. Furthermore, two pre-BPS Calcite 4–cemented fractures also fall in the latter "pre-BPS cluster" that covers oxygen values between −3.91 and −2.74‰VPDB and carbon values between +0.08 and +2.34‰VPDB. This cluster thus is somewhat depleted in oxygen and carbon values with respect to marine Cretaceous calcites.

However, some samples plot outside the main cluster. One grainstone matrix sample has a carbon value of −1.75‰VPDB. We interpret this value as being due to contamination with post-LPSS Calcite 9 cement that occurs among the early matrix cements of Lithotype III. Another sample corresponds to the cement filling a gastropod mold, which consists dominantly of Calcite 4. It possesses an oxygen value of −6.13‰VPDB and a carbon value of +2.54‰VPDB.

Post-LPSS Calcite 5 cement in fractures displays a trend toward more depleted oxygen values (−4.39 to −9.19‰ VPDB), while the carbon signature falls to −0.07 ± 1.64‰ VPDB. One analysis of a fracture filled with Calcite 6 and 7 cement possesses an oxygen signature of −6.93‰ VPDB

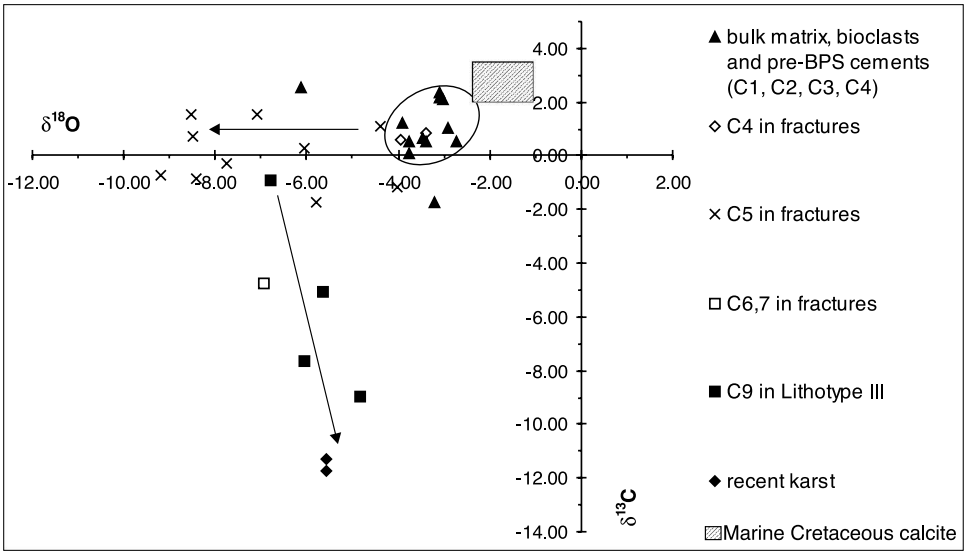

Figure 6. Stable isotope results for the Peñuela outcrop samples. The shaded rectangle indicates the signature of marine Cretaceous calcites, based on Czerniakowski et al. (1984), Swennen and Dusar (1996), and Frank and Arthur (1999).

and a remarkably lower carbon signature (−4.73‰ VPDB) with respect to Calcite 5. Calcite 9 sampled from vugs and biomolds in Lithotype III also displays a trend toward negative carbon values (as low as −8.99‰ VPDB), with oxygen values varying, at approximately −5.82 ± 0.98‰ VPDB. Two samples of recent karst (speleothem) cement plot with the lowest carbon values of −11.30 and −11.74‰ VPDB and an oxygen value of −5.58‰ VPDB.

FLUID INCLUSIONS

Special attention was paid to the presence of fluid inclusions in the matrix and fracture-filling cements for a microthermometric study to help the interpretation of the diagenetic history and the type and origin of involved fluids. Unfortunately, only small (1–4 μm) and monophase inclusions have been found in the studied wafers of Calcite 2 to 5 and Calcite 9 cements. The monophase inclusions, moreover, did not give rise to the creation of a vapor bubble when subjected to repeated heating-cooling cycles. These observations, however, argue for homogenization (and, consequently, precipitation) temperatures probably no higher than 50°C (Sabouraud et al., 1980), which is in agreement with thermal modeling results (Ortuño-Arzate et al., 2003).

DISCUSSION

Sedimentary Environment

During the Turonian-Santonian, global sea-level changes led to a decrease in the rate of relative sea-level rise (Vail et al., 1977), engendering a reestablishment of the ''old'' (as during Early Cretaceous) carbonate platform. The lower (Turonian) part of the Guzmantla Formation still indicates an outer-platform environment, while the Coniacian-Santonian Guzmantla deposits point out shallow-platform conditions characterized by an inner platform with isolated rudist patch reefs and shallow lagoons (Ortuño-Arzate et al., 2003). Similar Cretaceous platform deposits are described by Simo et al. (1993).

The shaly beds and (laminated) mudstones with few and restricted fauna (Lithotype I, basal part of the cycles) represent an open to protected lagoonal environment with low water energy (Wilson, 1975; Flügel, 1982; Bay and Bebout, 1983; Lehmann et al., 1999) or can be interpreted as somewhat deeper subtidal deposits with low water energy. However, the fenestral fabric, the restricted fauna, and the occurrence of stromatolites is indicative of a shallow intertidal environment, rather than deeper subtidal conditions. Therefore, we interpret the environment as a shallow, open to restricted lagoon. The intercalations of lag deposits in these mud-rich lithologies can be interpreted as related to intertidal channels. The middle part of the cycle groups wackestones to packstones with a varied fauna, local accumulations of debris from nearby rudist buildups, and some burrowed horizons. These deposits are interpreted as a shallow open platform or lagoonal environment with low to moderate energy. Intercalations of mudstones to wackestones with only foraminifera and gastropods point to somewhat more restricted episodes. Shell-debris horizons with mostly rudist shells coated by algae also indicate shallow deposition. The coarse-grained, diversified bioclastic grainstones with mainly coated or micritized, well-rounded and well-sorted carbonate grains (Lithotype III, upper part of the cycles) represent high-energy banks (shoals). Such a setting is also supported by the presence of isopachous, acicular calcite cements surrounding grains (Calcite 1). This is typical of early marine cementation in high-energy deposits (see ''Lithologic and Early Diagenesis Control on Oil-stained Porosity''). In the Peñuela quarry, typical rudist patch-reef deposits are lacking. Reef debris, however, is abundantly present.

At least two upward-coarsening cycles crop out in the Peñuela quarry. They reflect a low-energy, shallow, open to restricted lagoon environment during deposition of the basal package, grading into a higher-energy, more open, shallow lagoonal environment and culminating as high-energy shoal deposits. They can thus be regarded as upward-shoaling cycles evolving from a restricted to open lagoon receiving reef debris, toward reef-neighboring shoals. Alternatively, the cycles can be interpreted in another way, with the lowest-energy deposits forming the top of the sequence. In this situation, the low-energy deposits can be interpreted as more protected lagoonal deposits behind the shoal banks. The subsequent open-platformal wackestones to packstones then reflect a new transgressive pulse with increasing water circulation and reestablishment of open-marine conditions. The cycle finally culminates in high-energy shoals overlain by deposits of a more protected environment. These interpretations are equivocal, since only two cycles were studied in the outcrop.

Diagenetic History

The micrite coating of carbonate particles provides evidence of early marine diagenesis associated

with boring activities of microorganisms (Bathurst, 1966; Perry, 1999). The Calcite 1 cement is interpreted as an early marine, synsedimentary cement (Kendall and Tucker, 1973; Moore, 2001). This is based on the crystal morphology of the isopachous acicular calcite fringes (Shinn, 1969) lining inter- and intraparticle pore spaces and its occurrence as first-cement generation and its nonluminescent aspect.

The subsequent equant calcite cements (Calcite 2 to 4) are typical of meteoric to burial realms (Bathurst, 1971; Harris et al., 1985; Tucker, 1993). During the meteoric stage, unstable carbonate mineralogies also were dissolved or subjected to neomorphic alteration. The dissolution phase after Calcite 2 thus implies a change in water chemistry after a certain equilibration of the carbonate-water system. The meteoric origin of Calcite 3 is supported by the concentric-zoned non- and bright-to-dull-yellow luminescence pattern (NBD sequence; Meyers, 1978). The change in luminescence is related to varying redox conditions, from an oxidizing to reducing environment (Walkden and Berry, 1984; Machel, 1985; Barnaby and Rimstidt, 1989; Machel and Burton, 1991; Kaufmann et al., 1999). Another argument supporting a meteoric nature of the pore fluid is the occurrence of several minor dissolution episodes between different CL zones. The source of this meteoric fluid can be related to Upper Cretaceous local emersion of the platform in the Sierra Atoyac, about 15 km eastward from the Peñuela outcrops. This emersion episode is interpreted to relate to an early Laramide forebulge development and is associated with pre-BPS local karst development in the Atoyac area (Ferket et al., 2000; Ortuño-Arzate et al., 2003). Mechanical and chemical compaction affected the rocks during subsequent burial. The zoned Calcite 3 cement was partly dissolved locally before precipitation of Calcite 4. Calcite 4 possesses a dull luminescent pattern and is interpreted as pressure-dissolution-related cement, based on its petrographic relationship with compaction phenomena (i.e., rehealing of fractured particles and cements).

The stable isotope results of pre- and syn-BPS cements, bulk matrix analyses, and pre-BPS cemented fractures plot together in one cluster that is depleted only slightly with respect to a marine Cretaceous carbon value. For oxygen, the shift toward more depleted values is more pronounced. Because neither the acicular Calcite 1–cemented matrices nor the rudist shells have preserved their marine value, isotopic re-equilibration must be assumed. This re-equilibration may relate to recrystallization or neomorphic alteration (Prezbindowski, 1985) during burial, whereby the $\delta^{13}C$ signature is more or less retained, while the $\delta^{18}O$ signature decreases as a result of diagenetic alteration, perhaps at more elevated temperatures. However, recrystallization as a result of interaction with meteoric water, which is more depleted in oxygen than seawater, also can be invoked and could explain the slight $\delta^{13}C$ depletion caused by involvement of soil-derived CO_2 (Lohmann, 1987). This concurs with the observed NBD-luminescence succession of the pre-BPS cements. The origin of such fluids can be related to the pre-BPS emersion episode in the Atoyac area, which was caused by an early Laramide forebulge development (Ortuño-Arzate et al., 2003).

Pre-BPS fractures are cemented by a uniform, dull-luminescent calcite cement (Calcite 4) and also plot dominantly in this ''pre-BPS cluster,'' arguing for host-rock buffering during shallow burial. Carbonate is derived here from redistribution, possibly in relation to pressure-dissolution in compaction-sensitive intervals (Morse and Mackenzie, 1993; Heydari, 2000).

Mechanical compaction of the rocks led to broken and squeezed particles and to fracturing of earlier formed cements, which are subsequently rehealed, especially by Calcite 4. Chemical compaction involves pressure-dissolution with reprecipitation of calcite (i.e., Calcite 4, e.g., Matter, 1974; Buxton and Sibley, 1981; Merino et al., 1983) and engendered sutured grain boundaries in grain-supported lithologies, dissolution seams in argillaceous limestones, and stylolites (Meyers, 1980; Railsback, 1993; Bathurst, 1995). These compaction-related stylolites formed parallel to bedding. The timing of their development can be constrained about the beginning of the Paleocene, based on kinematic modeling (Ortuño-Arzate et al., 2003).

Tectonic shortening, i.e., layer-parallel shortening (LPS), in carbonate rocks is accommodated by the development of LPS stylolites (Whitaker and Bartholomew, 1999). LPS stylolites form early during Laramide deformation of the foreland (see above, ''*Post-BPS/pre- to syn-LPSS Diagenesis*''), immediately before folding and thrusting of the strata, i.e., during the Paleocene, according to kinematic modeling (Ortuño-Arzate et al., 2003). With respect to reservoir quality, it is important to note that these stylolites may have been opened during subsequent folding of the strata, whereby fluid migration was made possible along these former permeability barriers (Van Geet et al., 2002). Evidence of fluid flow along stylolites is also found in the oil-filled biomoldic to

vuggy porosity that developed adjacent to stylolites in Lithotypes I and II and which is related to a post-LPSS dissolution phase (D3).

Isotopic analyses of the post-LPSS Calcite 5 cement in fractures indicate a trend toward depleted oxygen values, while the carbon signature still remains more or less within the range of the host rock. This shift in $\delta^{18}O$ with respect to the host rock most probably reflects temperature fractionation. Evidence for this interpretation is provided from the study of other outcrops in the Cordoba Platform, where fractures are more abundant and their related fluid history better documented. Hydraulic fractures, arguing for overpressures, are common in the post-BPS/pre- to syn-LPSS period. Such fracture generations, however, have not been found in the Peñuela outcrop. Higher temperature fluids circulated along these fractures (based on depleted oxygen values that fell as low as −13‰VPDB and precipitation of saddle dolomite). In this period, fluids were expelled during tectonic compression. After LPSS development, again, lower-temperature fluids (with less depleted oxygen values) circulated along fractures. These fractures can be related to thrust emplacement (Ortuño-Arzate et al., 2003, and unpublished results). The Calcite 5 cement shows a broad range of depleted $\delta^{18}O$ values, probably reflecting cooling of expelled formation water moving upward along fractures. The cathodoluminescence of Calcite 5 is uniform dull luminescent, similar to and thus in equilibrium with the host rock.

The post-LPSS dissolution phase (D3) was responsible not only for dissolution along stylolites, but it generated enlarged inter- and intraparticular pores, as well as biomolds in the permeable Lithotype II strata. This dissolution phase is followed by the precipitation of Calcite 6 that occurs also along stylolites and in fractures cutting through Calcite 5 cemented fractures and by oil migration. This dissolution is thus interpreted to postdate Calcite 5. The change in cathodoluminescence characteristics indicates a change in fluid chemistry. One fracture cemented with Calcite 6 and 7 has been analyzed. It possesses a more depleted (−4.39‰VPDB) carbon signature than Calcite 5. Therefore, the dissolution and subsequent precipitation of Calcite 6 are interpreted as related to a meteoric fluid coming in after early exposure of the strata. The carbon depletion then can be explained by isotopically light, soil-derived CO_2 (Cerling, 1984; Lohmann, 1987). Alternatively, the dissolution can be related to a corrosive fluid preceding oil migration. The negative carbon value then can be interpreted in relation to oil maturation. In any event, this post-LPSS dissolution affected mainly the most permeable Lithotype II strata, thereby enhancing the reservoir capacity prior to oil migration.

Late-stage (telogenetic) dissolution is supported by outcrop and petrographic observations. Some of these features, such as the development of large vugs, biomolds, and even cavern porosity filled with internal sediment and/or several types of calcite cement, indicate karst development. Stable isotope results also suggest meteoric dissolution and karst development. The trend of Calcite 9 toward very depleted carbon signatures implies addition of soil-derived light carbon (Cerling, 1984; Lohmann, 1987). The most depleted carbon values come from recent speleothem cement. The depleted oxygen signatures of post-LPSS cements also can be explained by a meteoric origin, rather than by temperature fractionation. Otherwise, more depleted values would be more likely.

Lithologic and Early Diagenesis Control on Oil-stained Porosity

The different lithotypes underwent a different cementation and compaction history through time. Finer lithologies developed better reservoir characteristics with respect to oil-filled pores than the bioclastic grainstones. These observations suggest that sedimentary fabric controls porosity preservation and/or porosity development. This lithologic control differs from the classical scenario in which primary interparticle porosity and secondary moldic porosity development characterize the coarsest lithologies (i.e., grainstones; e.g., Bay and Bebout, 1983; Aqrawi et al., 1998; Madi et al., 2000; Budd, 2001).

In the mud-dominated Lithotype I, water circulation was insufficient to cement the small pores, leading to cement-poor lithologies. Here, compaction strongly reduced porosity and permeability during burial, but structural reactivation and subsequent dissolution along the many stylolites explain the oil impregnation in Lithotype I.

Porosity was reduced in Lithotype III, as a result of pervasive marine and meteoric cementation. Synsedimentary marine cementation is favored by high-energy environments such as shoals (e.g., Minero, 1991; Tucker, 1993). The original sediment is highly porous, and lime mud is washed out. Important volumes of water thus can circulate through the pore system. Since large volumes of water are needed to fill pore space entirely with marine cement

(Tucker, 1993; Moore, 2001), the cementation potential depends on water energy.

Lithotype II with pelletal micrite between the grains was deposited in medium-energy intertidal conditions in an open-platform lagoon. Interparticle pores are an order of magnitude smaller than in the well-sorted Lithotype III strata. Water movement, consequently, was slower, causing water volumes flushed through the sediments to be lower, resulting in less pervasive cementation than in Lithotype III (Tucker, 1993; Moore, 2001). Cementation also was favored in larger pores, while smaller pores remained open (e.g., Putnis and Mauthe, 2001). This led to limited early-marine and meteoric cementation in grain-supported intervals where the interparticular cements formed a rigid structure, so that the pore network was (partially) preserved. Consequently, micrite compaction was hindered. However, in more mud-dominated intervals, early-marine cements were less developed, so that burial compaction affected the rocks.

The pervasively oil-impregnated intervals correspond with the early cemented (stabilized) rocks of Lithotype II. The cement possesses a ''framework-stabilizing effect,'' enabling preservation of reservoir potential (Bay and Bebout, 1983; Feazel and Schatzinger, 1985; Swennen et al., 2000). These rocks still allow fluid flow, whereby cementation or secondary porosity development can occur. From petrographic observations, it is clear that dissolution affected the strata after LPSS development. The importance of LPSS opening and the subsequent creation of an open fluid flow already has been mentioned. Fluid flow preferentially occurred along open fractures and joint planes, as well as along open LPS stylolites and the interconnected matrix-pore network. Capillary forces can aid migration along porous heterogeneities (Bethke et al., 1991), thereby further enhancing porosity. Subsequently, oil migration (starting during the Eocene or later) filled up these pores.

Nonoil-stained Pores

Appreciable modern matrix porosity (intragranular pores, biomolds, and vugs) is observed in Lithotype III. These pores, however, are not oil-impregnated. Petrographic observations indicate that this secondary porosity was created after oil migration. This porosity development is linked to meteoric water infiltration and karst development in relation to post-orogenic uplift of the study area. However, it should be expected that the oil present in Lithotype II strata would have migrated, thereby filling the newly created pores in Lithotype III strata. The high viscosity of the oil and the lack of driving forces caused by the low temperature and water-saturated strata might explain the observations. The oil thus remained in situ, i.e., residual.

Lithotype III was seemingly more sensitive to this telogenetic karstic dissolution than Lithotypes I and II. This is explained by the oil-impregnated fine-grained nature of the Lithotype II rocks, which were less susceptible to the penetration of karstic fluids (Lomando, 1992). Lithotype I strata were less affected, because they were severely compacted. The pure grainstones, however, were more easily dissolved. Large bioclasts in Lithotype III have been preferentially dissolved. However, aragonite components probably would not have survived early and meteoric-burial diagenesis. A possible explanation is the preservation of isolated intragranular porosity that became connected after Laramide deformation as a result of the development/opening of joints and microfractures related to pressure-release during denudation of the area. Telogenetic karst fluids following these permeable pathways (LPSS, joint planes, fractures) connect these pores, forming a 3-D network of open structural features (leading to channel porosity) and matrix pores (biomoldic and vug porosity). The fact that these structural-controlled pathways were not filled with oil can be explained by the lack of driving forces and capillary forces at the moment of their reactivation/opening.

In the M. R. Aguilar 1A Well, similar selective oil impregnation in wackestones to packstones has been identified. Here, grainstones are generally not oil-impregnated, except along LPSS planes and where large dissolution vugs occur. Since the oil in the subsurface can migrate farther upward when secondary porosity is created, post-LPSS pores will increase the reservoir capacity of such lithologies.

Porosity-permeability Evolution

A schematic pathway for the evolution of porosity and permeability through time in the function of lithotypes is proposed in Figure 7. Here, porosity and permeability in the different lithotypes are placed into the fluid-deformation history. The pattern focuses on matrix porosity and consequently does not account for the development of fracture porosity that affected all lithotypes. The pattern tends to explain the selective oil migration in Lithotype II. Normally, the rate of porosity loss is expected to be lowest in the grainstones and highest in the finer lithologies (e.g., Bay and Bebout, 1983;

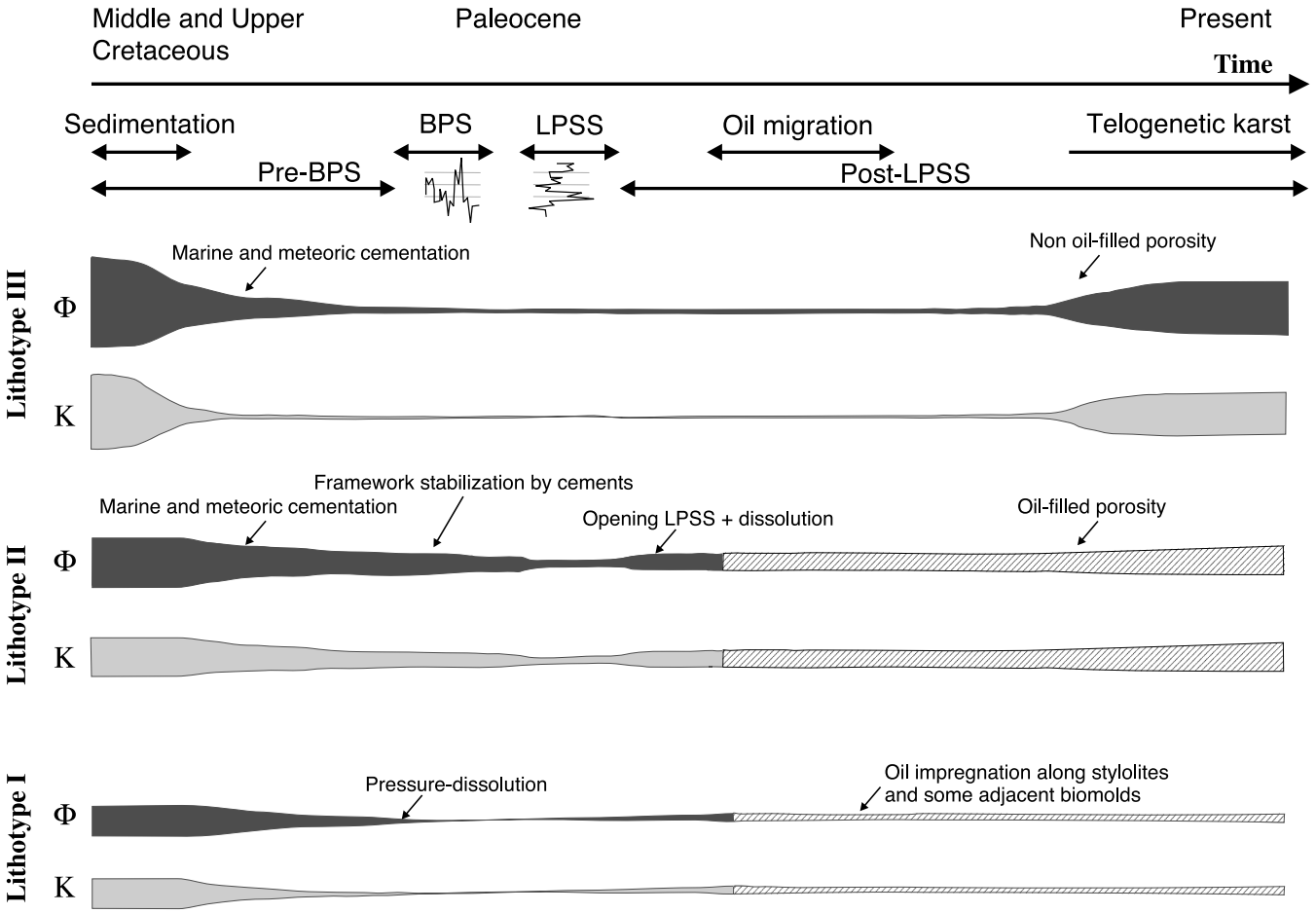

Figure 7. Relative porosity (Φ)-permeability (K) evolution pattern in the different lithotypes through time.

Aqrawi et al., 1998; Madi et al., 2000; Budd, 2001), whereas the Peñuela case study shows the reverse with regard to oil-filled pores. It is, however, not an exception or a local phenomenon, since selective oil impregnation in bioclastic wackestones to packstones also has been recognized in cores in the eastern buried front (e.g., M.R. Aguilar 1A Well). There, the strata are oil producing, and oil-filled secondary dissolution cavities have been observed. In the Peñuela surface analogue, the oil migration stopped before the important telogenetic karst development. However, if karst-related pores develop in the subsurface, they can form excellent oil reservoirs, as is the case in the successful Golden Lane field of Mexico (Coogan et al., 1972).

Although most fractures are cemented, some are still open and are filled with oil. They form mainly vertical fluid-migration pathways and act as (vertical) porosity-permeability conduits connecting with the porous matrix intervals. As such, they have the same effect on reservoir connectivity as opened LPS features and create a 3-D pore network. These observations stress the importance of the double matrix-fracture porosity of the reservoirs.

CONCLUSIONS

The Peñuela quarry forms an excellent outcrop analogue for subsurface time-equivalent reservoirs in the Cordoba Platform, of the Veracruz Basin. It allows the study of the spatial (3-D) porosity network and of factors controlling the porosity distribution.

The sedimentary environment of these rocks has been interpreted as an inner, shallow platform with isolated rudist patch reefs and lagoons. Two 20-m-scaled shoaling-upward cycles have been differentiated. Based on sedimentological, diagenetic, porosity, and oil impregnation characteristics, three lithotypes have been identified. Coarse, bioclastic grainstones (Lithotype III) deposited in high-energy shoal banks are pervasively cemented by early-marine and meteoric cements. Mud-dominated lithologies (Lithotype I) have undergone severe compaction, reducing porosity and permeability. Bioclastic wackestones to

packstones (Lithotype II), however, preserved appreciable matrix porosity as a result of framework-stabilizing cementation. During later diagenesis, porosity was even further enhanced as a result of dissolution by meteoric waters, allowing Lithotype II strata to attain the best reservoir quality. This scenario deviates from more common settings, in which grainstones normally preserve the best reservoir qualities.

The grainstones, however, possess at present a good, modern, karst-related porosity. In the Peñuela quarry, these karst cavities have not been filled with oil, because of the viscous nature of the residual oil. In the subsurface, however, this porosity network may be important. The finer-grained lithologies did not undergo this telogenetic secondary porosity enhancement, because the pore network was occluded by oil. In the mudstones, this is caused by the absence of any matrix porosity in relation to compaction.

The main porosity-controlling factors that have surfaced in this study are (1) the sedimentary environment, which influences the early and thus the later diagenetic evolution; (2) stylolite development (compactional as well as tectonic), which either reduces the porosity and permeability through pressure-dissolution and cementation or enhances the porosity and permeability by channeling undersaturated fluids; and (3) fracturing of the strata and the degree of cement-filling and tectonic opening.

ACKNOWLEDGMENTS

We are grateful to Miguel Espinoza, Juan Toriz, Ricardo Caraveo, and Martín Martínez for their help in organizing the field work in the Cordoba–Veracruz area. We would like to thank H. Nijs for the thin-section preparation and Professor M. Joachimski (University of Erlangen, Germany) and his collaborators for the isotope analyses.

The scanning electron microscopy study is supported by grant no. 2.0038.91 of the National Fund of Scientific Research of Belgium.

REFERENCES CITED

AlAasm, I. S., and K. K. Azmy, 1996, Diagenesis and evolution of microporosity of Middle-Upper Devonian Kee Scarp reefs, Normall Wells, Northwest Territories, Canada: Petrographic and chemical evidence. AAPG Bulletin, v. 80, p. 82–100.

Andrews, L. M., and L. B. Railsback, 1997, Controls on stylolite development: Morphologic, lithologic, and temporal evidence from bedding-parallel and transverse stylolites from the US Appalachians: Journal of Geology, v. 105, p. 59–73.

Aqrawi, A. A. M., G. A. Tehni, G. H. Sherwani, and B. M. A. Kareem, 1998, Mid-Cretaceous rudist-bearing carbonates of the Mishrif Formation: An important reservoir sequence in the Mesopotamian Basin, Iraq: Journal of Petroleum Geology, v. 21, p. 57–82.

Averbuch, O., D. Frizon de Lamotte, and C. Kissel, 1992, Magnetic fabric as a structural indicator of the deformation path within a fold-thrust structure: A test case from the Corbières (NE Pyrenees, France): Journal of Structural Geology, v. 14, p. 461–474.

Barnaby, R. J., and J. D. Rimstidt, 1989, Redox conditions of calcite cementation interpreted from Mn and Fe contents of authigenic calcites: Geological Society of America Bulletin, v. 101, p. 795–804.

Bathurst, R. C. G., 1966, Boring algae, micrite envelopes and lithification of molluscan biosparites: Geological Journal, v. 5, p. 89–109.

Bathurst, R. C. G., 1971, Carbonate cements and their diagenesis, *in* Developments in Sedimentology, v. 12: Amsterdam-Oxford-New York, Elsevier Scientific Publishing Co., 620 p.

Bathurst, R. C. G., 1995, Burial diagenesis of limestones under simple overburden— stylolites, cementation and feedback: Bulletin Société Géologique de France, v. 166, p. 181–192.

Bay, A. R., and D. G. Bebout, 1983, Cyclic, shoaling-carbonate banks in the Lower Glen Rose Formation (Cretaceous), South Texas, *in* Carbonate buildups— a core workshop: Society for Sedimentary Geology (SEPM) Workshop 4, p. 429–462.

Bethke, C. M., J. D. Reed, and D. F. Oltz, 1991, Long-range petroleum migration in the Illinois Basin: AAPG Bulletin, v. 75, p. 925–945.

Budd, D. A., 2001, Permeability loss with depth in the Cenozoic carbonate platform of west-central Florida: AAPG Bulletin, v. 85, p. 1253–1272.

Buxton, T. J., and D. F. Sibley, 1981, Pressure-solution features in a shallow buried limestone: Journal of Sedimentary Petrology, v. 51, p. 19–26.

Cerling, T. E., 1984, The stable isotopic composition of modern soil carbonate and its relationship to climate: Earth and Planetary Science Letters, v. 71, p. 229–240.

Coogan, A. H., D. G. Bebout, and C. Maggio, 1972, Depositional environments and geologic history of Golden Lane and Poza Rica trend, Mexico, an alternate view. AAPG Bulletin, v. 56, p. 511–518.

Czerniakowski, L. A., K. C. Lohmann, and J. L. Wilson, 1984, Closed-system marine burial diagenesis— isotopic data from the Austin chalk and its components: Sedimentology, v. 31, p. 863–877.

Dix, G. R., and H. T. Mullins, 1992, Shallow-burial diagenesis of deep-water carbonates, northern Bahamas: Results from deep-ocean drilling transects: Geological Society of America Bulletin, v. 104, p. 303–315.

Ehrenberg, S. N., E. B. Nielsen, T. A. Svana, and L.

Stemmerik, 1998, Diagenesis and reservoir quality of the Finnmark carbonate platform, Barents Sea: Results from wells 7128/6-1 and 7128/4-1: Norsk Geologisk Tidsskrift, v. 78, p. 225–251.

Feazel, C. T., and R. A. Schatzinger, 1985, Prevention of carbonate cementation in petroleum reservoirs, *in* N. Schneidermann and P. M. Harris, eds., Carbonate Cements: Society for Sedimentary Geology (SEPM) Special Publication No. 36, p. 97–106.

Ferket, H., F. Roure, R. Swennen, and S. Ortuño, 2000, Fluid migration placed into the deformation history of fold-and-thrust belts: An example from the Veracruz basin (Mexico). Journal of Geochemical Exploration, v. 69–70, p. 275–279.

Flügel, E., 1982, Microfacies analysis in limestones: Berlin, Heidelberg, New York, Springer-Verlag, 633 p.

Frank, D., and M. A. Arthur, 1999, Tectonic forcings of Maastrichtian ocean-climate evolution: Paleoceanography, v. 14, p. 103–117.

Frank, T. D., and K. Bernet, 2000, Isotopic signature of burial diagenesis and primary lithological contrasts in periplatformal carbonates (Miocene, Great Bahama Bank): Sedimentology, v. 47, p. 1119–1134.

Harris, P. M., C. G. St. C. Kendall, and A. Lerche, 1985, Carbonate cementation— a brief review, in N. Schneidermann and P. M. Harris, eds., Carbonate cements: Society for Sedimentary Geology (SEPM) Special Publication 36, p. 79–95.

Heydari, E., 2000, Porosity loss, fluid flow and mass transfer in limestone reservoirs: Application to the Upper Jurassic Smackover Formation, Mississippi: AAPG Bulletin, v. 84, p. 100–118.

Hendry, J. P., C. Taberner, J. D. Marshall, C. Pierre, and P. F. Carey, 1999, Coral reef diagenesis records porefluid evolution and paleohydrology of a siliciclastic basin margin succession (Eocene South Pyrenean foreland basin, northeastern Spain): Geological Society of America Bulletin, v. 111, p. 395–411.

James, N. P., and P. W. Choquette, 1990, Limestones— the sea floor diagenetic environment, in I. A. McIlreath and D. W. Morrow, eds., Diagenesis: Geoscience Canada Reprint series 4, p. 13–34.

Kaufmann, B., M. Schauer, and C. Reinhold, 1999, Concentric-zoned calcite cements of Middle Devonian carbonate mounds of the Mader Basin (eastern Anti-Atlas, Morocco)— a combined cathodoluminescence and microprobe study: Neues Jahrbuch Geologie und Paläontologie, Abhandlugen, Munchen, v. 214, p. 95–110.

Kendall, A. C., and M. E. Tucker, 1973, Radiaxial fibrous calcite: A replacement after acicular carbonate: Sedimentology, v. 20, p. 365–389.

Lehmann, C., D. A. Osleger, I. P. Montanez, W. Sliter, A. Arnaud-Vanneau, and J. Banner, 1999, Evolution of Cupido and Coahuila carbonate platforms, Early Cretaceous, Northeastern Mexico: Geological Society of America Bulletin, v. 111, p. 1010–1029.

Logan, B. W., and V. Semeniuk, 1976, Dynamic metamorphism: Processes and products in Devonian carbonate rocks, Canning Basin, Western Australia: Geological Society of Australia Special Publication No. 6, 138 p.

Lohmann, K. C., 1987, Geochemical patterns of meteoric diagenetic systems and their application to studies of paleokarst, *in* N. P. James and P. W. Choquette, eds., Paleokarst: New York, Springer-Verlag, p. 58–80.

Lomando, A. J., 1992, The influence of solid reservoir bitumen on reservoir quality: AAPG Bulletin, v. 76, p. 1137–1152.

Longman, M. W., 1980, Carbonate diagenetic textures from nearsurface diagenetic environments: AAPG Bulletin, v. 64, p. 461–478.

Machel, H. G., 1985, Cathodoluminescence in calcite and dolomite and its chemical interpretation: Geoscience Canada, v. 12, p. 139–147.

Machel, H. G., and E. A. Burton, 1991, Factors governing cathodoluminescence in calcite and dolomite and their implications for studies of carbonate diagenesis, *in* C. E. Barker and O. C. Kopp, eds., Luminescence microscopy and spectroscopy: Qualitative and quantitative applications: Society for Sedimentary Geology (SEPM) Short Course No. 25, p. 37–57.

Madi, A., M. M. Savard, P. A. Bourque, and G. X. Chi, 2000, Hydrocarbon potential of the Mississippian carbonate platform, Bechar basin, Algerian Sahara: AAPG Bulletin, v. 84, p. 266–287.

Matter, A., 1974, Burial diagenesis of pelitic and carbonate deep-sea sediments from the Arabian Sea, *in* Initial Reports of the Deep Sea Drilling Project: Washington, D. C., U. S. Government Printing Office, v. 23, p. 241–470.

Merino, E., P. Ortolera, and P. Strickholm, 1983, Generation of evenly-spaced pressure-solution seams during (late) diagenesis: A kinetic theory: Contributions to Mineralogy and Petrology., 82, p. 360–370.

Meyers, W. J., 1978, Carbonate cements: Their regional distribution and interpretation in Mississipian limestones of southwestern New Mexico: Sedimentology, v. 25, p. 371–400.

Meyers, W. J., 1980, Compaction in Mississippian skeletal limestones, Southwestern New Mexico: Journal of Sedimentary Petrology, v. 50, p. 457–474.

Minero, C. J., 1991, Sedimentation and diagenesis along open and island-protected windward carbonate platform margins of the Cretaceous El Abra Formation, Mexico: Sedimentary Geology, v. 71, p. 261–288.

Mitra, G., 1994, Strain variation in thrust sheets across the Sevier fold-and-thrust belt (Idaho Utah Wyoming)— implications for section restoration and wedge taper evolution: Journal of Structural Geology, v. 16, p. 585–602.

Moore, C. H., 2001, Carbonate reservoirs: Porosity evolution and diagenesis in a sequence stratigraphic framework, *in* Developments in Sedimentology v. 55: Amsterdam, Elsevier Scientific Publishing Co., 444 p.

Morse, J. W., and F. T. Mackenzie, 1993, Geochemical

constraints on $CaCO_3$ transport in subsurface sedimentary environments: Chemical Geology, v. 105, p. 181–196.

Ortuño-Arzate, S., H. Ferket, M. C. Cacas, R. Swennen, and F. Roure, 2003, Late Cretaceous carbonate reservoirs in the Cordoba Platform and Veracruz Basin, Eastern Mexico, *in* C. Bartolini, R. T. Buffler, and J. Blickwede, eds., The Circum-Gulf of Mexico and the Caribbean: Hydrocarbon habitats, basin formation, and plate tectonics: AAPG Memoir 79, p. 476–514.

Perry, C. T., 1999, Biofilm-related calcification, sediment trapping, and constructive micrite envelopes: A criterion for the recognition of ancient grass-bed environments? Sedimentology, v. 46, p. 33–45.

Prezbindowski, D. R., 1985, Burial cementation— is it important? A case study, Stuart City Trend, South Central Texas, *in* N. Schneidermann and P. M. Harris, eds., Carbonate cements: Society for Sedimentary Geology (SEPM) Special Publication No. 36, p. 241–264.

Putnis, A., and G. Mauthe, 2001, The effect of pore size on cementation in porous rocks: Geofluids, v. 1, p. 37–41.

Railsback, L. B., 1993, Contrasting styles of chemical compaction in the Upper Pennsylvanian Dennis limestone in the Midcontinent region, USA. Journal of Sedimentary Petrology, v. 63, p. 61–72.

Railsback, L. B., and L. M. Andrews, 1995, Tectonic stylolites in the undeformed Cumberland Plateau of Southern Tennessee: Journal of Structural Geology, v. 17, p. 911–915.

Sabouraud, C., J. C. Macquar, and H. Ravier, 1980, Les inclusions fluides, témoins et faux-témoins des conditions de dépôt. Quelques exemples pris dans les minéralisations Pb, Zn, Ba, F du Sud du Massif Central français: Mineralogy Deposita, v. 15, p. 211–230.

Saller, A. H., D. A. Budd, and P. M. Harris, 1994, Unconformities and porosity development in carbonate strata: Ideas from a Hedberg Conference: AAPG Bulletin, v. 78, p. 857–872.

Saller, A. H., K. Lounsbury, and M. Birchard, 2001, Facies control on dolomitization and porosity in the Devonian Swan Hills Formation in the Rosevear area, west-central Alberta: Bulletin of Canadian Petroleum Geology, v. 49, p. 458–471.

Shinn, E. A., 1969, Submarine lithification of Holocene carbonate sediments in the Persian Gulf: Sedimentology, v. 12, p. 109–144.

Simo, J. A. T., R. W. Scott, and J. P. Masse, eds., 1993, Atlas of Cretaceous carbonate platforms: AAPG Memoir 56, 479 p.

Storti, F., F. Salvini, and K. McClay, 1997, Fault-related folding in sandbox analogue models of thrust wedges: Journal of Structural Geology, v. 19, p. 583–602.

Storti, F., and F. Salvini, 2001, The evolution of a model trap in the central Apennines, Italy: Fracture patterns, fault reactivation and development of cataclastic rocks in carbonates at the Narni Anticline: Journal of Petroleum Geology, v. 24, p. 171–190.

Sun, S. Q., A. E. Fallick, and B. J. P. Williams, 1992, Influence of original fabric on subsequent porosity evolution— an example from the Corallian (Upper Jurassic) reefal limestones, the Weald Basin, Southern England: Sedimentary Geology, v. 79, p. 139–160.

Swennen, R., and M. Dusar, 1996, Diagenesis of Late Cretaceous to Paleocene carbonates in the Rur Valley Graben (Molenbeersel borehole, NE Belgium). Annales de la Société Géologique du Nord, v. 5, p. 215–226.

Swennen, R., R. Muskha, and F. Roure, 2000, Fluid circulation in the Ionian fold and thrust belt (Albania): Implications for hydrocarbon prospectivity: Journal of Geochemical Exploration, v. 69, p. 629–634.

Tavarnelli, E., 1997, Structural evolution of a foreland fold-and-thrust belt: The Umbria-Marche Apennines, Italy: Journal of Structural Geology, v. 19, p. 523–534.

Tucker, M. E., 1993, Carbonate diagenesis and sequence stratigraphy, *in* V. P. Wright, ed., Sedimentology, Rev. 1: Oxford, Blackwell Scientific Publications, p. 51–72.

Tucker, M. E., and V. P. Wright, 1990, Carbonate sedimentology: Oxford, Blackwell Scientific Publications, 482 p.

Vail, P. R., R. M. Mitchum, and S. Thompson, 1977, Seismic stratigraphy and global changes of sea level, part 4: Global cycles of relative change of sea level, *in* C. E. Payton, ed., Seismic stratigraphy— applications to hydrocarbon exploration: AAPG Memoir 26, p. 83–87.

Van Geet, M., R. Swennen, C. Durmishi, F. Roure, and P. Muchez, 2002, Paragenesis of Cretaceous to Eocene carbonate reservoirs in the Ionian foreland fold and thrust belt (Albania): Relation between tectonism and fluid flow: Sedimentology, v. 49, p. 1–22.

Wachter, E., and J. M. Hayes, 1985, Exchange of oxygen isotopes in carbon dioxide– phosphoric acid systems: Chemical Geology, v. 52, p. 365–374.

Walkden, G. M., and J. R. Berry, 1984, Syntaxial overgrowths in muddy crinoidal limestones: Cathodoluminescence sheds new light on an old problem: Sedimentology, v. 31, p. 251–267.

Whitaker, A. E., and M. J. Bartholomew, 1999, Layer parallel shortening: A mechanism for determining deformation timing at the junction of the central and southern Appalachians: American Journal of Science, v. 299, p. 238–254.

Whitaker, F., P. Smart, Y. Hague, D. Waltham, and D. Bosence, 1999, Structure and function of a coupled two-dimensional diagenetic and sedimentological model of carbonate platform evolution: Society for Sedimentary Geology (SEPM) Special Publication No. 62, p. 337–355.

Wilson, J. L., 1975, Carbonate facies in Geologic History: Berlin, Heidelberg, Springer-Verlag, 471 p.